Eur. Phys. J. D (2012) 66: 284
DOI: 10.1140/epjd/e2012-30517-2

THE EUROPEAN PHYSICAL JOURNAL D

Colloquium

Application of the time-dependent close-coupling approach to few-body atomic and molecular ionizing collisions

J. Colgan[1,a] and M.S. Pindzola[2]

[1] Theoretical Division, Los Alamos National Laboratory, Los Alamos, 87545 NM, USA
[2] Department of Physics, Auburn University, Auburn, 36849 AL, USA

Received 21 August 2012 / Received in final form 20 September 2012
Published online 20 November 2012 –

Abstract. We review the recent progress made in applying the time-dependent close-coupling approach to ionizing collisions of electrons, photons, and ions with small atoms and molecules. The last twenty years have seen a proliferation of non-perturbative approaches applied to fundamental atomic and molecular scattering processes. Such processes form the building blocks of describing the dynamics of plasmas over a wide range of temperatures and densities, and also provide insight into the long-range Coulomb interactions between charged particles. Studies of the few-body Coulomb problem presented in electron, photon, or ion-impact ionization of small atoms and molecules, by direct solution of the time-dependent Schrödinger equation, are particularly useful because the complicated three-body boundary conditions of more than one continuum particle in a Coulomb potential are not required. With the continuing growth and increasing availability of high-performance computing resources, such methods can now be applied to a wide variety of scattering processes. The recent progress made using such a time-dependent approach is described in this colloquium. In this paper, we focus on the recent results obtained for one-, two-, and three-electron systems, thus building on a previous review of the time-dependent close-coupling method [M.S. Pindzola et al., J. Phys. B **40**, R39 (2007)], which also described the application to multi-electron targets.

1 Introduction

A time-dependent approach to solving the Schrödinger equation for two electrons in the continuum removes the need for an asymptotic boundary condition for the two-electron wavefunction in order to extract scattering information. The difficulty of the two-electron continuum boundary condition was first pointed out by Rudge and Seaton [1] and Peterkop [2]. The important advantage afforded by a time-dependent approach was first realized by Bottcher [3,4], and was followed by early studies [5,6] of electron scattering from hydrogen. Several *s*-wave (zero angular momenta) studies were also subsequently performed [7–9]. Since then, the development of the time-dependent close-coupling approach generalized to treat an arbitrary number of angular momenta [10] has allowed progress on many ionization processes found in atomic collision physics.

The need for a non-perturbative approach to few-body atomic and molecular collisions grew more pressing as impressive new technologies were applied to such reactions. In particular, multiple coincidence measurements, the use of a magnetic-optical-trap (MOT), and the cold target recoil ion momentum spectroscopy (COLTRIMS) technique [11] all contributed to new and ever more precise measurements of the scattering properties of atomic collision systems. Although previous perturbative techniques, and many variants on these, were often adequate at high impact energies, or for highly charged systems, it was long recognized that perturbative approaches are inaccurate when the three-body interaction between particles becomes important. This occurs at low impact energies, and for neutral (or near-neutral) targets, where the electron-electron potential is of the same order as the electron-nuclear potential, and when the outgoing electrons have enough time to interact and exchange energy.

In the last twenty years many novel non-perturbative approaches have been applied to few-body atomic and molecular collisions. The *R*-matrix approach, first pioneered by Burke and collaborators [12,13], has been widely used in the calculation of electron-impact excitation and photoionization cross sections. It has been particularly useful in computing the large datasets required for astrophysical purposes, such as the atomic data needed to calculate accurate opacities of iron. This approach was extended to treat electron-impact ionization problems, and also excitation cross sections where coupling to the continuum is important, by inclusion of pseudo-states in the *R*-matrix expansion [14,15]. Such *R*-matrix with pseudo-states (RMPS) approaches have now been applied to a wide variety of scattering problems, and semi- and fully-relativistic versions of RMPS methods are available.

[a] e-mail: jcolgan@lanl.gov

Recently, the R-matrix with pseudostates approach has been extended to examine electron-impact ionization of small molecular targets [16]. A hyperspherical R-matrix approach using semiclassical outgoing waves (HRM-SOW) was applied to double photoionization of He in the early 2000s [17,18]. It has also been used to examine double photoionization of Be [19].

The convergent close-coupling (CCC) approach was first applied to electron-hydrogen scattering in the early 1990s [20] and has since been extensively applied to electron-helium scattering [21–23] as well as electron scattering from a range of alkali atoms [24]. The CCC approach was applied to double photoionization of He in the mid 1990s [25–27] and has since explored double photoionization processes in other small atoms and ions, such as Be [28] and Li [29,30]. More recently, the CCC approach has also been applied to antiproton impact ionization of H and He [31,32].

An exterior complex-scaling (ECS) approach was first proposed as a solution to the three-body problem of the electron-impact ionization of hydrogen in the late 1990s [33,34]. It was very successful in reproducing a wide range of measured angular distributions for this ionization process. More recently, the ECS method was applied to the double photoionization of He [35] and also molecular hydrogen [36,37]. It has also been extended to examine two-photon double ionization processes in He and H_2 [38,39].

The time-dependent close-coupling (TDCC) approach discussed in this review differs fundamentally from these previous non-perturbative approaches in that it solves the time-dependent, rather than time-independent, Schrödinger equation. It thus avoids the need to appeal to a final-state boundary condition in order to extract scattering information. For three-body Coulomb problems, the boundary condition of two electrons moving in the field of a charged third body has long been known to be notoriously difficult to deal with, although recent progress has been made in recasting the problem into a somewhat more tractable solution [40,41]. The TDCC approach takes advantage of the rapid advances made in high-performance computing resources to efficiently solve the discretized Schrödinger equation for two (or more) electrons moving in the field of a charged nucleus (or nuclei). In the following sections we provide a detailed description of the application of the TDCC approach to electron-impact ionization, (multiple) photoionization, and ion-impact ionization of small atoms and molecules, work that has been ongoing for now many years. We provide a presentation of the pertinent coupled equations that need to be solved for the problem under consideration, and show how scattering information may be extracted by suitable projection methods. We then discuss some of the resulting cross sections and angular distributions for a variety of scattering processes, and briefly show how these calculations can shed some insight on the underlying physical picture governing the scattering events. Atomic units are used unless otherwise stated. We end with a short conclusion and discuss future plans and challenges.

2 Electron-impact ionization of small atoms and molecules

2.1 Single ionization of small atoms

The time-dependent Schrödinger equation for electron scattering from a one-electron atom of nuclear charge Z can be written as

$$i\frac{\partial\Psi(\boldsymbol{r}_1,\boldsymbol{r}_2,t)}{\partial t} = H_{\rm atom}(\boldsymbol{r}_1,\boldsymbol{r}_2)\Psi(\boldsymbol{r}_1,\boldsymbol{r}_2,t), \tag{1}$$

where the time-independent Hamiltonian is given by

$$H_{\rm atom}(\boldsymbol{r}_1,\boldsymbol{r}_2) = \sum_{i=1}^{2}\left(-\frac{1}{2}\nabla_i^2 - \frac{Z}{r_i}\right) + \frac{1}{|\boldsymbol{r}_1-\boldsymbol{r}_2|}. \tag{2}$$

By taking advantage of the spherical symmetry of atoms, the total wavefunction for the two electrons may be expanded in coupled spherical harmonics and projected onto the time-dependent Schrödinger equation to obtain the following set of partial differential equations for each LS symmetry:

$$\begin{aligned} i\frac{\partial P^{LS}_{l_1l_2}(r_1,r_2,t)}{\partial t} &= T_{l_1l_2}(r_1,r_2)P^{LS}_{l_1l_2}(r_1,r_2,t) \\ &\quad + \sum_{l_1'l_2'} V^{L}_{l_1l_2,l_1'l_2'}(r_1,r_2)P^{LS}_{l_1'l_2'}(r_1,r_2,t), \end{aligned} \tag{3}$$

where

$$T_{l_1l_2}(r_1,r_2) = \sum_{i=1}^{2}\left(-\frac{1}{2}\frac{\partial^2}{\partial r_i^2} + \frac{l_i(l_i+1)}{2r_i^2} - \frac{Z}{r_i}\right) \tag{4}$$

and the coupling operator is given by

$$\begin{aligned} &V^{L}_{l_1l_2,l_1'l_2'}(r_1,r_2) \\ &\quad = (-1)^{l_1+l_1'+L}\sqrt{(2l_1+1)(2l_1'+1)(2l_2+1)(2l_2'+1)} \\ &\quad\times \sum_{\lambda}\frac{(r_1,r_2)^{\lambda}_{<}}{(r_1,r_2)^{\lambda+1}_{>}}\begin{pmatrix} l_1 & \lambda & l_1' \\ 0 & 0 & 0\end{pmatrix}\begin{pmatrix} l_2 & \lambda & l_2' \\ 0 & 0 & 0\end{pmatrix}\begin{Bmatrix} l_1 & l_2 & L \\ l_2' & l_1' & \lambda\end{Bmatrix}, \end{aligned} \tag{5}$$

where $r_<(r_>) = \min(\max)(r_1,r_2)$. If we wish to consider electron scattering from multi-electron atoms, we must add a potential term to the single particle operator $T_{l_1l_2}(r_1,r_2)$ of equation (4). For example, for electron scattering from helium, the extra potential terms can be written as the sum of a "direct" potential term V_D, given by

$$V_D(r) = \int_0^{\infty}\frac{P^2_{1s}(r_1)}{\max(r_1,r)}\,dr_1 \tag{6}$$

and an "exchange" potential term V_X. One option for the V_X potential is a semiempirical local potential [42] defined as

$$V_X(r) = -\alpha_s\left(\frac{24\rho_{1s}(r)}{\pi}\right)^{1/3}. \tag{7}$$

Here, $P_{1s}(r)$ is a frozen-core radial orbital calculated as the hydrogenic ground state radial orbital of He^+, α_s is

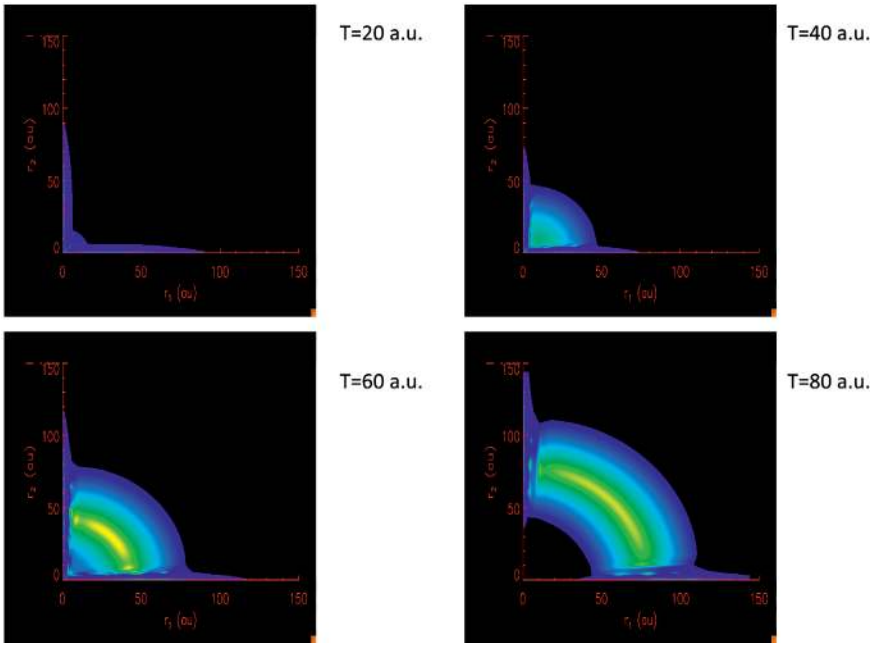

Fig. 1. Radial probability densities, summed over all channels, at four different times as indicated for electron scattering from He. The probability densities are indicated by the colours ranging from yellow (maximum) to blue (minimum).

an adjustable parameter and $\rho_{1s}(r) = P_{1s}^2/4\pi r^2$ is the radial probability density of the core electron. Other options for the exchange potentials can also be used. For electron scattering from targets with more than two electrons, one can employ l-dependent pseudo-potentials [10] to represent the interaction of the target electrons with the outgoing electrons.

The two-electron radial functions of equation (3) at time $t = 0$ are constructed as

$$P_{l_1 l_2}^{LS}(r_1, r_2, t = 0) = \sqrt{\frac{1}{2}}\big[G_{k_0 l_1}(r_1) P_{n l_2}(r_2) + (-1)^S P_{n l_1}(r_1) G_{k_0 l_2}(r_2)\big], \quad (8)$$

where k_0 is the linear momentum and $G_{k_0 l}(r)$ is a Gaussian radial wave packet of energy $E_0 = k_0^2/2$, with $P_{nl}(r)$ a bound radial wavefunction for a one-electron atom. The coupled equations (3) are then propagated according to the usual time-dependent close-coupling prescription, for each LS symmetry. Our standard computational approach is to partition the (r_1, r_2) coordinates of the two-dimensional radial wavefunctions and all operators over the processors of a parallel computer. One can employ explicit or implicit time propagators to solve these close-coupled equations [10]. We have found that explicit methods are more efficient for calculations of electron scattering from atoms, even though a smaller time step is required compared to the implicit method. An example of the radial probability density obtained from a TDCC calculation of electron scattering from He at an incident energy of 64.6 eV is shown in Figure 1. The radial wavefunction squared, summed over all $l_1 l_2 LS$ channels, is shown at four different times during the propagation of equation (3). We observe how the wavefunction flux moves away from the origin (where the nucleus is located). The dominant feature at early times is a concentration of probability density along the box boundaries; this represents elastic scattering of the incident electron, and also some electron-impact excitation of the target. At later times, we find significant flux near the $r_1 = r_2$ line, which represents ionization of the target. As time gets larger and the ionization process continues, this flux moves away from the nucleus.

At an appropriate time $t = T$ after the collision, in which only outgoing waves are present in each channel, the wavefunction in momentum space for each LS symmetry is given by

$$P_{l_1 l_2}^{LS}(k_1, k_2, T) = \int_0^\infty dr_1 \int_0^\infty dr_2 P_{k_1 l_1}(r_1) P_{k_2 l_2}(r_2) \times P_{l_1 l_2}^{LS}(r_1, r_2, t = T), \quad (9)$$

where $P_{kl}(r)$ are appropriately normalized single particle continuum channels. These are Coulomb waves for scattering from a one-electron target, or distorted waves if scattering from a multi-electron target is considered. We remind the reader that equation (9) is a suitable approach to extracting the ionizing amplitudes when the time-dependent equations are propagated to sufficiently long times, and when a sufficiently large radial mesh is employed.

The total ionization cross section can be found by summing the square of this wavefunction over all $l_1 l_2$ coupled channels and over all LS terms, for all possible excess energies:

$$\sigma_{\rm ion} = \frac{w_t}{l_t + 1} \frac{\pi}{4k_0^2} \int_0^\infty dk_1 \int_0^\infty dk_2 \sum_{LS} (2L + 1)(2S + 1) \times \sum_{l_1 l_2} \left| P_{l_1 l_2}^{LS}(k_1, k_2, T) \right|^2, \quad (10)$$

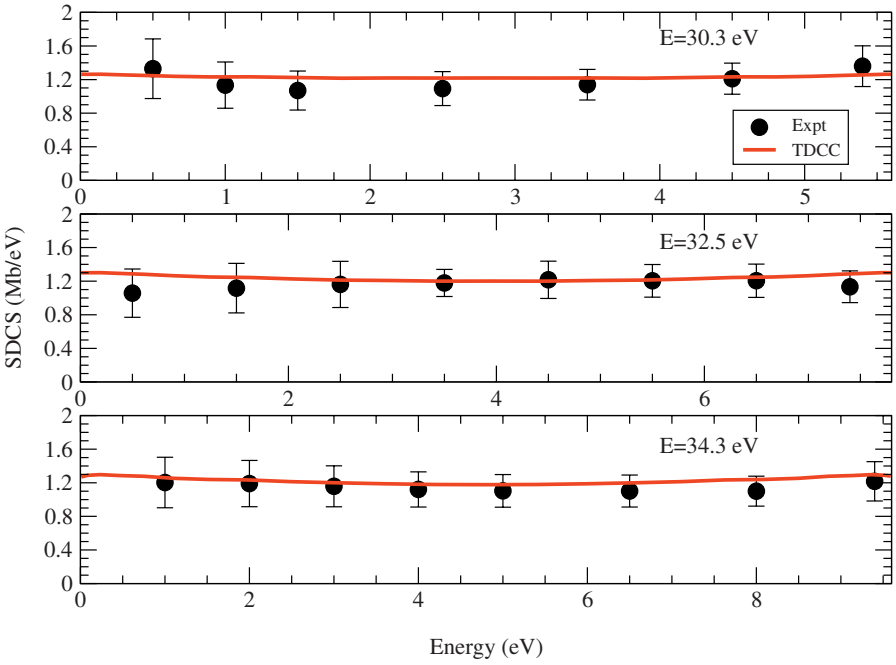

Fig. 2. Single differential cross sections as a function of E_1, the energy of the first electron, for electron-impact single ionization of helium at various incident electron energies as labeled. We compare with the measurements of [72].

where w_t is the occupation number of the initial state (e.g. 1 for H and 2 for He) with angular momentum l_t.

One of the earliest TDCC applications was to electron scattering from atomic hydrogen [5,6]. Total ionization cross sections were found to be in very good agreement with absolute measurements [43] and with other non-perturbative calculations [44–46]. This good agreement between non-perturbative approaches also exists for excited-state H [47] as well as the hydrogenic ions He^+ [48] and Li^{2+} [49]. Total single ionization cross sections for He computed using the TDCC approach [50,51] were also found to be in good agreement with several sets of measurements [52,53], and total ionization cross sections from excited-state He have also been reported [54].

In support of the atomic data needs of fusion and astrophysical modelers, multiple TDCC calculations have been performed for a variety of neutral atoms and ions. Total ionization cross sections were presented for Li^+ [55], and also for neutral Li in its ground [56] and excited states [57]. Ionization cross sections for all ion stages of Be have been calculated [58,59], as well as B [60,61]. Carbon [62] and the ground and excited states of C^+ [63,64] have also been examined. Single ionization cross sections have been reported for Ne in its ground [62] and excited [65] states, as well as Mg [66], Mg^+ [67], and the neutral and first few ionized stages of Al [66–68]. It is also straightforward to extract probabilities for excitation from TDCC calculations. Electron-impact excitation cross sections for Li have been calculated [69,70] and for several ion stages of Be [71]. Good agreement is generally found with R-matrix with pseudo-state calculations.

The momentum space wavefunction given by equation (9) also allows us to define cross sections differential in energy and/or angle of the outgoing electrons. The single differential (in energy) cross section (SDCS) is defined as

$$\frac{d\sigma}{dE_1} = \frac{w_t}{l_t+1}\frac{\pi}{4k_0^2}\frac{1}{k_1k_2}\sum_{L,S}(2L+1)(2S+1) \times \int_0^\infty dk_1 \int_0^\infty dk_2\, \delta\left(\alpha - \tan^{-1}\frac{k_2}{k_1}\right) \times \sum_{l_1l_2}\left|P^{LS}_{l_1l_2}(k_1,k_2,T)\right|^2, \quad (11)$$

where E_1 is the energy of one of the outgoing electrons (with the energy of the remaining electron defined through energy conservation), and α is the angle in the hyperspherical plane between the two outgoing momenta vectors k_1 and k_2. The SDCS for electron-impact ionization of helium for several impact energies is presented in Figure 2 [51]. The SDCS is compared with absolute measurements from the CSU Fullerton group [72]. The agreement between the calculations and measurements is excellent. At these low impact energies, the SDCS exhibits a flat shape. At larger impact energies, the SDCS becomes more 'U'-shaped [51], which is a result of the preference of one of the outgoing electrons to carry away most of the excess energy.

The triple differential cross section (TDCS) is given by

$$\frac{d^3\sigma}{dE_1 d\Omega_1 d\Omega_2} = \frac{w_t}{l_t+1}\frac{\pi}{4k_0^2}\frac{1}{k_1k_2}\sum_{S}(2S+1) \times \int_0^\infty dk_1 \int_0^\infty dk_2\, \delta\left(\alpha - \tan^{-1}\frac{k_2}{k_1}\right) \times \left|\sum_L i^L\sqrt{2L+1}\sum_{l_1l_2}(-i)^{l_1+l_2}e^{i(\sigma_{l_1}+\sigma_{l_2})} \times P^{LS}_{l_1l_2}(k_1,k_2,T)\mathcal{Y}_{l_1l_2}(\hat{k}_1,\hat{k}_2)\right|^2, \quad (12)$$

where in this case α is the angle in the hyperspherical plane between the two outgoing momenta vectors k_1 and k_2, $\mathcal{Y}_{l_1 l_2}(\hat{k}_1, \hat{k}_2)$ is a coupled spherical harmonic defined as

$$\mathcal{Y}_{l_1 l_2}\left(\hat{k}_1, \hat{k}_2\right) = \sum_{m_1 m_2} C^{l_1 l_2 L}_{m_1 m_2 M} \times Y_{l_1 m_1}(\theta_1, \phi_1) Y_{l_2 m_2}(\theta_2, \phi_2) \quad (13)$$

and σ_l is the Coulomb phase shift. If scattering from a multi-electron target is considered, one must also include the distorted-wave phase shift in equation (12). Double differential cross sections in energy and angle may be obtained by integrating the triple differential cross section over one of the outgoing electron solid angles Ω.

Double and triple differential cross sections for electron-impact ionization of H have been calculated for various incident electron energies and a range of outgoing electron angles and energies [73,74]. Generally good agreement is found between the TDCC calculations and measurement, and also with CCC and ECS non-perturbative calculations. For electron-impact single ionization of He, TDCC calculations have also been completed for a wide range of electron kinematics [51,75–78] and compared with a variety of experimental results, as well as CCC calculations and perturbative distorted-wave calculations. The TDCC results generally agree very well with almost all of the experimental data.

Figure 3 shows an example of the comparison between the TDCC calculations and the measurements made by the Manchester group [76]. The geometries employed by the Manchester group are unique in that a movable incident electron "gun" is used, with the outgoing electrons detected in a plane. The results shown in Figure 3 are for equal energy outgoing electrons as a function of the angle ξ, where 2ξ is the angle between the outgoing electrons, all for different gun angles ψ. This out-of-plane geometry is markedly different from the more standard $(e, 2e)$ TDCS measurements, which are often made for coplanar geometries (all electrons lie in a common plane), where the detection angle of one electron is fixed and the cross section measured as a function of the second electron angle. The Manchester detection geometries are highly symmetric, with only singlet channels contributing to the TDCS, and revealed an unexpected deep minimum in early measurements [79] of the TDCS from He. This feature is not linked to selection rules or electron-electron repulsion, which is often the cause of zeros in the TDCS in other related problems. The deep minimum is well reproduced by the TDCC calculations (where the relative measurements are normalized to the TDCC calculations), and further analysis [76] shows that interference between the contributing partial waves is linked to the deep minimum feature. Recently, the presence of a vortex in the two-electron continuum wavefunction [80,81] was postulated as a further reason for this unexpected minimum in this cross section.

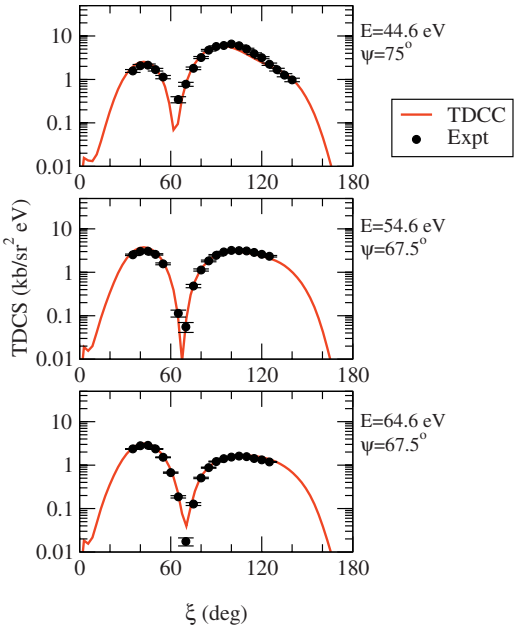

Fig. 3. Triple differential cross sections for electron-impact single ionization of helium at three incident electron energies as labeled, for equal energy sharing outgoing electrons. The calculations were made at different gun angles ψ of the Manchester experimental set-up, where the gun angle is the angle between the incident electron beam and the plane in which the outgoing electrons (separated by an angle 2ξ) move. We compare with the relative measurements of [79], which are normalized to the TDCC calculations at the peak of the cross section.

2.2 Single ionization of small molecules

Application of the TDCC approach to electron-impact ionization of diatomic molecules has been explored in recent years. Since diatomic molecules break the spherical symmetry that was exploited in TDCC studies of atomic ionization, we choose to now expand the total electronic wavefunction over rotation functions ϕ, with the remaining coordinates (r, θ) discretized on a lattice [10]. This choice requires significantly more computational resources for electron-molecule calculations compared to the electron-atom calculations, since one must now represent the four coordinates $(r_1, \theta_1, r_2, \theta_2)$ on a grid in the molecular case, compared to the two coordinates (r_1, r_2) that are represented on a grid in the atomic case.

However, the basic structure of TDCC calculations for electron-molecule scattering is quite similar to the atomic case. We solve the same time-dependent Schrödinger equation as represented in equation (1), but in the molecular case the Hamiltonian is now given by

$$H_{\rm mol} = \sum_{i=1}^{2} \left(-\frac{1}{2}\nabla_i^2 - \sum_{\pm} \frac{Z}{\sqrt{r_i^2 + \frac{1}{4}R^2 \pm r_i R \cos\theta_i}} \right) + \frac{1}{|\boldsymbol{r}_1 - \boldsymbol{r}_2|}, \quad (14)$$

where R is the internuclear distance, and Z is the charge on each nucleus. The total electronic wavefunction is expanded in rotational functions for each total angular momentum projection about the internuclear axis, M, and total spin angular momentum, S:

$$\Psi^{MS}(\boldsymbol{r}_1,\boldsymbol{r}_2,t) = \sum_{m_1m_2} \frac{P^{MS}_{m_1m_2}(r_1,\theta_1,r_2,\theta_2,t)}{r_1r_2\sqrt{\sin\theta_1}\sqrt{\sin\theta_2}} \times \Phi_{m_1}(\phi_1)\Phi_{m_2}(\phi_2), \quad (15)$$

where $\Phi_m(\phi) = \frac{e^{im\phi}}{\sqrt{2\pi}}$ and $M = m_1 + m_2$. Upon substitution of Ψ into the time-dependent Schrödinger equation, we obtain the following set of time-dependent close-coupled partial differential equations for each MS symmetry [10,82]:

$$i\frac{\partial P^{MS}_{m_1m_2}(r_1,\theta_1,r_2,\theta_2,t)}{\partial t} = T_{m_1m_2}(r_1,\theta_1,r_2,\theta_2) \times P^{MS}_{m_1m_2}(r_1,\theta_1,r_2,\theta_2,t) + \sum_{m_1'm_2'} V^{M}_{m_1m_2,m_1'm_2'}(r_1,\theta_1,r_2,\theta_2) \times P^{MS}_{m_1'm_2'}(r_1,\theta_1,r_2,\theta_2,t), \quad (16)$$

where

$$T_{m_1m_2}(r_1,\theta_1,r_2,\theta_2) = \sum_{i=1}^{2}\left(K(r_i) + K(r_i,\theta_i) + \frac{m_i^2}{2r_i^2\sin^2\theta_i} - \sum_{\pm}\frac{Z}{\sqrt{r_i^2 + \frac{1}{4}R^2 \pm r_iR\cos\theta_i}}\right), \quad (17)$$

and K are kinetic energy operators [82]. The coupling operator is given by:

$$V^{M}_{m_1m_2,m_1'm_2'}(r_1,\theta_1,r_2,\theta_2) = \sum_{\lambda}\frac{(r_1,r_2)^{\lambda}_{<}}{(r_1,r_2)^{\lambda+1}_{>}}\sum_{q}\frac{(\lambda-|q|)!}{(\lambda+|q|)!} \times P^{|q|}_{\lambda}(\cos\theta_1)P^{|q|}_{\lambda}(\cos\theta_2) \times \int_0^{2\pi}d\phi_1\int_0^{2\pi}d\phi_2\,\Phi_{m_1}(\phi_1)\Phi_{m_2}(\phi_2) \times e^{iq(\phi_2-\phi_1)}\Phi_{m_1'}(\phi_1)\Phi_{m_2'}(\phi_2), \quad (18)$$

where $P^{|q|}_{\lambda}(\cos\theta)$ is an associated Legendre function. As in the atomic case, if we wish to consider multi-electron molecular targets, we must add potential terms to the single particle operator $T_{m_1m_2}(r_1,\theta_1,r_2,\theta_2)$ of equation (17). For electron scattering from H_2, these additional potential terms can be represented by direct and exchange potential contributions [83], in a similar way to which the electron scattering from He was calculated, as discussed earlier.

The initial condition for the solution of the TDCC equations (Eq. (16)) for electron scattering from a one-electron homonuclear diatomic molecule may be given by:

$$P^{MS}_{m_1m_2}(r_1,\theta_1,r_2,\theta_2,t=0) = \sqrt{\frac{1}{2}}\big[G_{k_0l_0m_1}(r_1,\theta_1)P_{nlm_2}(r_2,\theta_2) + (-1)^S P_{nlm_1}(r_1,\theta_1)G_{k_0l_0m_2}(r_2,\theta_2)\big], \quad (19)$$

where $P_{nlm}(r,\theta)$ is a bound radial and angular wavefunction for a one-electron molecule, and $G_{k_0l_0m}$ is a Gaussian wavepacket for an incident energy $k_0^2/2$ and angular momentum l_0. It was found that implicit time propagation methods [10] were more efficient in the molecular case, compared to an explicit time propagator. This is due to the need for a very small time step in the explicit time propagation due to the discretization of the orbital angular momentum on the grid. The implicit propagator can employ much larger time steps, and is more efficient even though the matrix inversions required by an implicit method make each time step slower than the explicit approach.

The total ionization cross section for the electron single ionization of a one-electron molecule is given by:

$$\sigma_{\rm ion} = \frac{w_t}{l_t+1}\frac{\pi}{4k_0^2}\int_0^{\infty}dk_1\int_0^{\infty}dk_2\sum_{S}\sum_{l_0}\sum_{M}\sum_{l_1l_2}\sum_{m_1m_2} \times (2S+1)\left|P^{l_0MS}_{l_1m_1l_2m_2}(k_1,k_2,T)\right|^2, \quad (20)$$

where $P^{l_0MS}_{l_1m_1l_2m_2}(k_1,k_2,T)$ is the wavefunction which results after projection of the four-dimensional radial and angular wavefunctions onto products of one-electron continuum states after propagation to a suitable time T, given by

$$P^{l_0MS}_{l_1m_1l_2m_2}(k_1,k_2,T) = \int_0^{\infty}dr_1\int_0^{\pi}d\theta_1\int_0^{\infty}dr_2\int_0^{\pi}d\theta_2 \times P_{k_1l_1|m_1|}(r_1,\theta_1)P_{k_2l_2|m_2|}(r_2,\theta_2) \times P^{l_0MS}_{m_1m_2}(r_1,\theta_1,r_2,\theta_2,t=T). \quad (21)$$

TDCC calculations for the electron-impact ionization of H_2^+ [82] were found to be in excellent agreement with measurements [84]. For electron-impact ionization of H_2 [83], TDCC calculations were also in good agreement with measurement [85] as well as with RMPS calculations [16]. More recently, TDCC calculations have also been performed for electron-impact ionization of the larger molecule Li_2 [86].

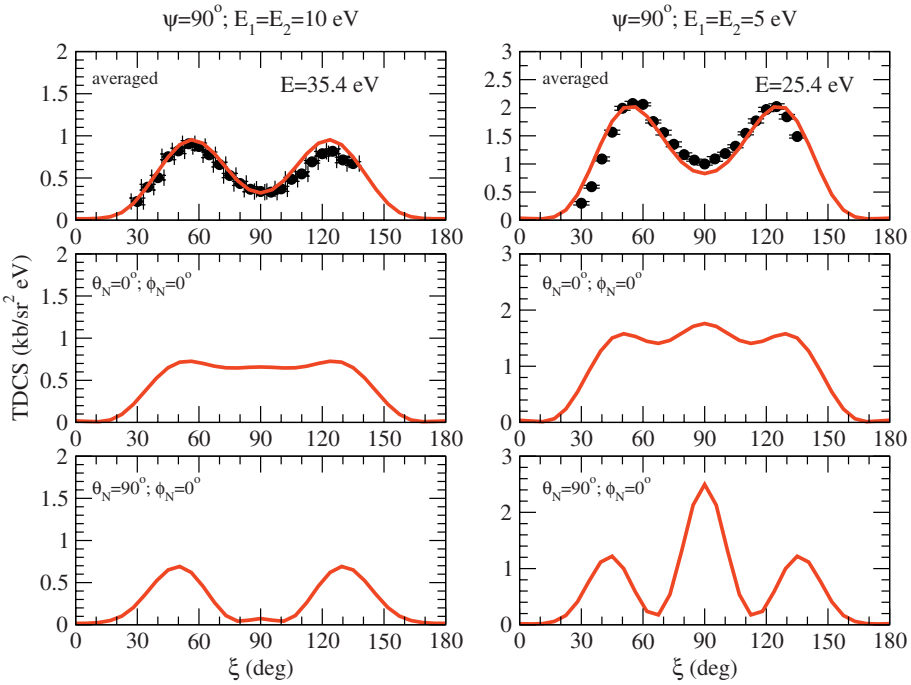

Fig. 4. Triple differential cross sections for electron-impact single ionization of H_2 at two incident electron energies as labeled, for equal energy sharing outgoing electrons [88]. The calculations were made at a gun angle $\psi = 90°$ (i.e. the perpendicular geometry) of the Manchester experimental set-up. The upper panels compare the relative measurements [87] (which are normalized to the calculations) with TDCC calculations averaged over all orientations. The lower panels show TDCC calculations made at specific orientations as indicated: middle panels show calculations made at $(\theta_N = 0°, \phi_N = 0°)$, along the z-axis, and the lower panels show calculations made at $(\theta_N = 90°, \phi_N = 0°)$, perpendicular to the z-axis.

As in atomic ionization, we may define energy and angular differential cross sections for molecular ionization. The single differential cross section for electron-impact ionization of a diatomic molecule can be written as

$$\frac{d\sigma}{dE_1} = \frac{w_t}{l_t+1}\frac{\pi}{4k_0^2}\frac{1}{k_1 k_2}\sum_S (2S+1) \times \int_0^\infty dk_1 \int_0^\infty dk_2\, \delta\left(\alpha - \tan^{-1}\frac{k_2}{k_1}\right) \times \sum_{l_0}\sum_{M=-l_0}^{+l_0}\sum_{l_1 l_2}\sum_{m_1 m_2}\left|P^{l_0 MS}_{l_1 m_1 l_2 m_2}(k_1,k_2,T)\right|^2. \quad (22)$$

The triple differential cross section may be expressed as

$$\frac{d^3\sigma}{dE_1 d\Omega_1 d\Omega_2} = \frac{w_t}{l_t+1}\frac{\pi}{4k_0^2}\frac{1}{k_1 k_2}\sum_S (2S+1) \times \int_0^\infty dk_1 \int_0^\infty dk_2\, \delta\left(\alpha - \tan^{-1}\frac{k_2}{k_1}\right)|\mathcal{M}|^2, \quad (23)$$

where k_0 is the incident electron's momentum and k_1 and k_2 are the outgoing electron momenta (ejected into solid angles $\Omega_{1,2}$). For diatomic molecules, where the z-axis is defined along the internuclear direction, and the incoming electron beam is oriented at angles (θ_k, ϕ_k) with respect to the z-axis,

$$\mathcal{M} = \sum_{l_0}\sum_{M=-l_0}^{+l_0} i^{l_0} Y^*_{l_0 M}(\theta_k,\phi_k) \times \sum_{l_1 l_2}\sum_{m_1 m_2}(-i)^{l_1+l_2}\, e^{i(\sigma_{l_1}+\sigma_{l_2})} \times P^{l_0 MS}_{l_1 m_1 l_2 m_2}(k_1,k_2,T) Y_{l_1 m_1}(\hat{k}_1) Y_{l_2 m_2}(\hat{k}_2)\delta_{m_1+m_2,M}. \quad (24)$$

Our TDCS expression defined by equations (23) and (24) is given in the molecular frame. To compare with experiment, a transformation must be made into the Laboratory frame. The TDCS for molecular ionization is dependent on the angles between the incoming electron beam and the molecular axis, or equivalently, to the angle between the molecular axis and the outgoing electrons. This dependence has no analogue in atomic ionization. The molecular orientation has been shown to have a strong effect on the TDCS, as was demonstrated recently for H_2 [76,87,88]. Figure 4 shows this dependence for two incident energy cases.

In the upper panels of Figure 4 we show H_2 TDCS measurements in the perpendicular plane for two sets of outgoing electron energies as indicated. The TDCC calculations are in excellent agreement with experiment and clearly show the central minimum found previously at

these energies [89,90]. In the middle and lower panels we present TDCC calculations for the same geometries where now the molecular orientation is fixed at $\theta_N = 0°$, $\phi_N = 0°$ and $\theta_N = 90°$, $\phi_N = 0°$, respectively. For cases where the molecule is aligned along the z-axis (i.e. along the incoming electron beam), the central minimum in the TDCS disappears. For the $E_1 = E_2 = 10$ eV case (left-hand-side of Fig. 4), the TDCS is flat in the central region, and at the lower energies a small maximum is found. The two side peaks (near $\xi = 60°$ and 120°) remain. This can be understood since the two outgoing electrons have little probability of colliding between the nuclei, since the initially bound electron is constrained by the fixed molecule position. The electron-electron collision is most likely to occur in a region where the attractive force from the nuclei is substantial, allowing greater backscatter and so a larger cross section in the $\xi = 90°$ region.

For cases where the molecule is perpendicular to the incoming beam ($\theta_N = 90°$, $\phi_N = 0°$, lower panels), the TDCS is quite different from the averaged case. For 10 eV outgoing electrons, the dip in the TDCS is very pronounced, but for the 5 eV outgoing electron case, this dip has turned into a maximum in the central region. At even lower energies (not shown), we find that this central peak completely dominates the cross section, resulting in a TDCS which is quite He-like. This trend appears to indicate that post-collision interaction (PCI) begins to influence the TDCS shape for the 5 eV outgoing electrons, and as the electron energy decreases, PCI dominates the shape of the TDCS. The electron-electron interaction pushes the electrons apart so that their preferred escape direction is back-to-back. This also suggests that the Wannier region may extend somewhat further out in energy for oriented molecules than was previously found for the randomly oriented molecular case [90]. Experimental investigations are in progress to measure the triple differential cross sections from oriented H_2.

2.3 Double ionization of small atoms

The TDCC approach has also been extended to treat three active electrons, which is required to calculate electron-impact double ionization of two-electron systems, as well as electron-impact ionization-excitation cross sections. Extension to three active electrons results in a significantly more complicated calculation compared to a two active electron case, as well as a much more computationally intensive problem. The complications are due to the large number of coupled channels which arise due to the coupling of three active electrons, which is also further complicated since the spatial and spin components of the three-electron wavefunction do not separate. This latter point also complicates the projection techniques used to extract probabilities for the many excitation and ionization processes now possible.

The time-dependent Schrödinger equation for electron scattering from a two-electron atom is given by:

$$i\frac{\partial \Psi(\boldsymbol{r}_1, \boldsymbol{r}_2, \boldsymbol{r}_3, t)}{\partial t} = H_{\rm atom}\Psi(\boldsymbol{r}_1, \boldsymbol{r}_2, \boldsymbol{r}_3, t), \qquad (25)$$

where the non-relativistic Hamiltonian for the scattering system is given by:

$$H_{\rm atom} = \sum_{i=1}^{3}\left(-\frac{1}{2}\nabla_i^2 - \frac{Z}{r_i}\right) + \sum_{i<j=1}^{3}\frac{1}{|\boldsymbol{r}_i - \boldsymbol{r}_j|}. \qquad (26)$$

The total electronic wavefunction is expanded in coupled spherical harmonics for each total orbital angular momentum, $\mathcal{L}$, and total spin angular momentum, $\mathcal{S}$:

$$\Psi^{\mathcal{LS}}(\boldsymbol{r}_1, \boldsymbol{r}_2, \boldsymbol{r}_3, t) = \sum_{l_1 l_2}\sum_{Ll_3}\frac{P^{\mathcal{LS}}_{l_1 l_2 L l_3}(r_1, r_2, r_3, t)}{r_1 r_2 r_3} \times \sum_{M m_3} C^{L\ \ l_3\ \ \mathcal{L}}_{M\ m_3\ 0} \sum_{m_1 m_2} C^{l_1\ l_2\ \ L}_{m_1 m_2 M} \times Y_{l_1 m_1}(\hat{r}_1) Y_{l_2 m_2}(\hat{r}_2) Y_{l_3 m_3}(\hat{r}_3). \qquad (27)$$

Upon substitution of Ψ into the time-dependent Schrödinger equation, we obtain the following set of time-dependent close-coupled partial differential equations for each $\mathcal{LS}$ symmetry [10,91]:

$$i\frac{\partial P^{\mathcal{LS}}_{l_1 l_2 L l_3}(r_1, r_2, r_3, t)}{\partial t} = T_{l_1 l_2 l_3}(r_1, r_2, r_3) P^{\mathcal{LS}}_{l_1 l_2 L l_3}(r_1, r_2, r_3, t) + \sum_{l_1' l_2' L' l_3'}\sum_{i<j=1}^{3} V^{\mathcal{L}}_{l_1 l_2 L l_3, l_1' l_2' L' l_3'}(r_i, r_j) P^{\mathcal{LS}}_{l_1' l_2' L' l_3'}(r_1, r_2, r_3, t), \qquad (28)$$

where

$$T_{l_1 l_2 l_3}(r_1, r_2, r_3) = \sum_{i=1}^{3}\left(-\frac{1}{2}\frac{\partial^2}{\partial r_i^2} + \frac{l_i(l_i+1)}{2r_i^2} - \frac{Z}{r_i}\right), \qquad (29)$$

and the $V^{\mathcal{L}}_{l_1 l_2 L l_3, l_1' l_2' L' l_3'}(r_i, r_j)$ are two-electron coupling operators [10].

The initial condition for the solution of the TDCC equations (Eq. (28)) for electron scattering from a two-electron atom may be given by:

$$P^{\mathcal{L}}_{l_1 l_2 L l_3}(r_1, r_2, r_3, t = 0) = \sum_{l_1', l_2'} \bar{P}^{L'}_{l_1' l_2'}(r_1, r_2) G_{k_0 l_3'}(r_3) \delta_{l_1, l_1'} \delta_{l_2, l_2'} \delta_{l_3, l_3'} \delta_{L, L'}, \qquad (30)$$

where $\bar{P}^{L'}_{l_1' l_2'}(r_1, r_2)$ with $L' = 0$ and $l_1' = l_2' = l$ are the ground-state radial wavefunctions for the two-electron atom, obtained by relaxation of the two-electron TDCC equations in imaginary time. Probabilities for all the many collision processes are obtained by $t \to \infty$ projection onto fully antisymmetric spatial and spin wavefunctions. As an example, for electron double ionization of the ground state of the helium atom, the partial collision probability

$$\mathcal{P}^{\mathcal{LS}}_{l_1 l_2 LS l_3}(k_1,k_2,k_3,t) = \Bigg| \sum_{L'} \delta_{L,L'} Q_a R(123,t) - \sum_{L'} (-1)^{l_2+l_3+L+L'} \sqrt{(2L+1)(2L'+1)} \begin{Bmatrix} l_2 & l_1 & L \\ l_3 & \mathcal{L} & L' \end{Bmatrix} Q_b R(132,t) - \sum_{L'} (-1)^{l_1+l_2-L'} \delta_{L,L'} Q_c R(213,t) + \sum_{L'} (-1)^{l_1+l_2+L} \sqrt{(2L+1)(2L'+1)} \begin{Bmatrix} l_2 & l_1 & L \\ l_3 & \mathcal{L} & L' \end{Bmatrix} Q_c R(312,t) + \sum_{L'} (-1)^{l_2+l_3+L'} \sqrt{(2L+1)(2L'+1)} \begin{Bmatrix} l_1 & l_2 & L \\ l_3 & \mathcal{L} & L' \end{Bmatrix} Q_b R(231,t) - \sum_{L'} \sqrt{(2L+1)(2L'+1)} \begin{Bmatrix} l_1 & l_2 & L \\ l_3 & \mathcal{L} & L' \end{Bmatrix} Q_a R(321,t) \Bigg|^2, \quad (31)$$

is given by:

see equation (31) above,

where

$$R(ijk,t) = \int_0^\infty dr_1 \int_0^\infty dr_2 \int_0^\infty dr_3 \times P_{k_1 l_1}(r_i) P_{k_2 l_2}(r_j) P_{k_3 l_3}(r_k) P^{\mathcal{L}}_{l_1 l_2 L' l_3}(r_1,r_2,r_3,t). \quad (32)$$

The $P_{kl}(r)$ are continuum radial wavefunctions for the He^+ atomic ion and,

$$Q_a = \sqrt{\frac{1}{2}}\delta_{S,0} - \sqrt{\frac{1}{6}}\delta_{S,1}, \quad Q_b = \sqrt{\frac{2}{3}}\delta_{S,1},$$
$$Q_c = -\sqrt{\frac{1}{2}}\delta_{S,0} - \sqrt{\frac{1}{6}}\delta_{S,1}, \quad \text{and} \quad \mathcal{S} = \frac{1}{2}.$$

To guard against the unwanted contribution to the partial collision probability coming from the continuum correlation part of the two-electron bound wavefunctions, one may project out the two-electron bound states from the three-electron time-propagated radial wavefunction and then project onto all electron momenta k_i. Alternatively, we found that a simple restriction of the sums over the electron momenta k_i, so that the conservation of energy,

$$E_{\text{atom}} + \frac{k_0^2}{2} = \frac{k_1^2}{2} + \frac{k_2^2}{2} + \frac{k_3^2}{2}, \quad (33)$$

was approximately conserved, greatly reduced contamination from the continuum piece of the two-electron bound wavefunctions. In addition, this method of restricted momenta sums should become more accurate as the lattice size increases.

The total cross section for electron double ionization of a two-electron atom is given by:

$$\sigma_{\text{dion}} = \frac{\pi}{2k_0^2} \int_0^\infty dk_1 \int_0^\infty dk_2 \int_0^\infty dk_3 \times \sum_{\mathcal{LS}} (2\mathcal{L}+1)(2\mathcal{S}+1) \times \sum_{LS} \sum_{l_1 l_2 l_3} \left| P^{\mathcal{LS}}_{l_1 l_2 LS l_3}(k_1,k_2,k_3,T) \right|^2, \quad (34)$$

where $P^{\mathcal{LS}}_{l_1 l_2 LS l_3}(k_1, k_2, k_3, T)$ is a three-electron momentum-space wavefunction obtained by projection of the coordinate-space wavefunctions at a final time T following equations (31) and (32). The first three-electron TDCC calculations, building on earlier model calculations [92], were performed for electron-impact double ionization of He [91] where the total double ionization cross sections were in good agreement with measurements made by the Belfast group [53]. Ionization-excitation total cross sections were also reported [91]. The double ionization cross sections were later extended to higher impact energies [93]. Total ionization cross sections were then calculated for electron-impact double ionization of H^- [94], and were able to distinguish between two sets of conflicting measurements, as shown in Figure 5. The TDCC calculations were in excellent agreement with the measurements of [95], and around a factor of 5 lower than the older measurements of [96]. Recently, the TDCC method has been used to calculate electron-impact double ionization of Be-like targets [97,98] and of Mg [99]. These calculations were made by including direct and local exchange potential operators in the one-electron terms given by equation (29) to represent the interaction of the frozen core with the active electrons.

As previously for single ionization, one can obtain energy and angular differential cross section for electron-impact double ionization. The double energy differential cross section for electron-impact double ionization

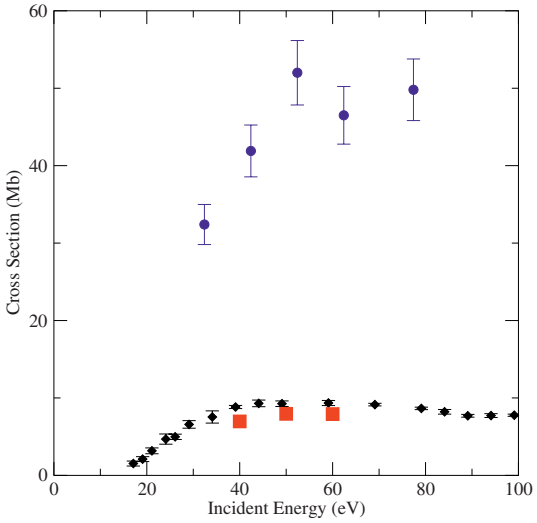

Fig. 5. Electron-impact double ionization cross section from H^-. The time-dependent close-coupling calculations (solid squares) [94] are compared with the measurements of [95] (diamonds) and of [96] (circles).

is given by:

$$\frac{d^2\sigma}{dE_2 dE_3} = \frac{\pi}{2k_0^2}\frac{1}{k_1 k_2 k_3\sqrt{k_1^2+k_2^2}}\sum_{\mathcal{LS}}(2\mathcal{L}+1)(2\mathcal{S}+1) \times \int_0^\infty dk_1 \int_0^\infty dk_2 \int_0^\infty dk_3 \times \delta\left(\alpha - \tan^{-1}\frac{k_2}{k_1}\right)\delta\left(\beta - \tan^{-1}\frac{k_3}{\sqrt{k_1^2+k_2^2}}\right) \times \sum_{l_1,l_2,l_3,L,S}\frac{1}{6}\sum_{ijk}^{6}|P^{\mathcal{LS}}_{l_1 l_2 L S l_3}(k_i,k_j,k_k,T)|^2, \quad (35)$$

where α is an angle in the (k_1, k_2) hyperspherical plane and β is an angle in the plane perpendicular to the (k_1, k_2) hyperspherical plane, both defined from 0 to $\frac{\pi}{2}$ radians.

The pentuple energy and angle differential cross section for electron-impact double ionization is given by:

$$\frac{d^5\sigma}{dE_2 dE_3 d\Omega_1 d\Omega_2 d\Omega_3} = \frac{\pi}{2k_0^2}\frac{1}{k_1 k_2 k_3\sqrt{k_1^2+k_2^2}} \times \sum_{\mathcal{S}}(2\mathcal{S}+1)\int_0^\infty dk_1 \int_0^\infty dk_2 \int_0^\infty dk_3 \times \delta\left(\alpha - \tan^{-1}\frac{k_2}{k_1}\right)\delta\left(\beta - \tan^{-1}\frac{k_3}{\sqrt{k_1^2+k_2^2}}\right) \times \sum_{S}\frac{1}{6}\sum_{ijk}^{6}\left|\sum_{\mathcal{L}} i^{\mathcal{L}}\sqrt{2\mathcal{L}+1} \times \sum_{l_1,l_2,l_3,L}(-i)^{l_1+l_2+l_3}\, e^{i(\sigma_{l_1}(k_i)+\sigma_{l_2}(k_j)+\sigma_{l_3}(k_k))} \times P^{\mathcal{LS}}_{l_1 l_2 L S l_3}(k_i,k_j,k_k,T)\mathcal{Y}_{l_1 l_2 L l_3 \mathcal{L}}(\Omega_i,\Omega_j,\Omega_k)\right|^2, \quad (36)$$

where σ_l is the Coulomb phase shift and $\mathcal{Y}_{l_1 l_2 L l_3 \mathcal{L}}$ is a coupled product of three spherical harmonics.

To date, only one set of calculations for the differential cross sections resulting from electron-impact double ionization of He has been reported [100], for an incident electron energy of 106 eV. The double energy differential cross sections were found to be qualitatively similar to the single energy differential cross sections calculated for single ionization. The pentuple angular differential cross sections (at equal energy sharing between all three outgoing electrons) were compared to recent reaction microscope measurements [101], and reasonable qualitative agreement was found. Further measurements are available at smaller impact energies [102], although TDCC calculations at such energies require large mesh sizes and propagation times for convergence.

3 Photoionization of small atoms and molecules

3.1 Single-photon double ionization of two-electron atoms

The time-dependent close-coupling method has been applied to numerous problems in double photoionization of two-electron atoms and molecules. Two formulations of the TDCC method for two-electron systems subject to an electromagnetic field have been given. The first formulation describes a two-electron atom in a strong time-varying electromagnetic field and the Schrödinger equation can be written as

$$i\frac{\partial\Psi(\boldsymbol{r}_1,\boldsymbol{r}_2,t)}{\partial t} = (H_{\rm atom}+H_{\rm rad})\Psi(\boldsymbol{r}_1,\boldsymbol{r}_2,t), \quad (37)$$

where the non-relativistic Hamiltonian for the atom is given by equation (2) and the Hamiltonian for a linearly polarized radiation field is given by:

$$H_{\rm rad} = E(t)\cos\omega t\sum_{i=1}^{2} r_i\cos\theta_i, \quad (38)$$

where $E(t)$ is the electric field amplitude and ω the radiation field frequency. Using similar expansions over coupled spherical harmonics as defined in Section 2.1, we obtain the following set of time-dependent close-coupled partial differential equations [103]:

$$i\frac{\partial P^{LS}_{l_1 l_2}(r_1,r_2,t)}{\partial t} = T_{l_1 l_2}(r_1,r_2)P^{LS}_{l_1 l_2}(r_1,r_2,t) + \sum_{l_1' l_2'} V^{L}_{l_1 l_2, l_1' l_2'}(r_1,r_2)P^{LS}_{l_1' l_2'}(r_1,r_2,t) + \sum_{L'}\sum_{l_1' l_2'} W^{LL'}_{l_1 l_2, l_1' l_2'}(r_1,r_2,t)P^{L'S}_{l_1' l_2'}(r_1,r_2,t), \quad (39)$$

where now

$$W^{LL'}_{l_1l_2,l'_1l'_2}(r_1,r_2,t) = \delta_{l_2,l'_2}(-1)^{l_2} \times \sqrt{(2l_1+1)(2l'_1+1)(2L+1)(2L'+1)} \times r_1E(t)\cos\omega t \begin{pmatrix} l_1 & 1 & l'_1 \\ 0 & 0 & 0 \end{pmatrix} \begin{pmatrix} L & 1 & L' \\ 0 & 0 & 0 \end{pmatrix} \begin{Bmatrix} l_1 & l_2 & L \\ L' & 1 & l'_1 \end{Bmatrix} + \delta_{l_1,l'_1}(-1)^{l_1} \sqrt{(2l_2+1)(2l'_2+1)(2L+1)(2L'+1)} \times r_2E(t)\cos\omega t \begin{pmatrix} l_2 & 1 & l'_2 \\ 0 & 0 & 0 \end{pmatrix} \begin{pmatrix} L & 1 & L' \\ 0 & 0 & 0 \end{pmatrix} \begin{Bmatrix} l_2 & l_1 & L \\ L' & 1 & l'_2 \end{Bmatrix}. \quad (40)$$

These equations are very similar to the strong-field equations solved by the Belfast group using the HELIUM code [104,105], where strong-field double ionization of He for high-intensity, long-wavelength radiation is examined.

Alternatively, the time-dependent wavefunction for a two-electron atom may be divided into two parts:

$$\Psi(\boldsymbol{r}_1,\boldsymbol{r}_2,t) = \psi_0(\boldsymbol{r}_1,\boldsymbol{r}_2)\,e^{-iE_0t} + \psi(\boldsymbol{r}_1,\boldsymbol{r}_2,t), \quad (41)$$

where ψ_0 is the exact eigenfunction and E_0 is the exact eigenenergy of the time-independent atomic Hamiltonian. Substitution into the time-dependent Schrödinger equation yields:

$$i\frac{\partial\psi(\boldsymbol{r}_1,\boldsymbol{r}_2,t)}{\partial t} = (H_{\rm atom}+H_{\rm rad})\psi(\boldsymbol{r}_1,\boldsymbol{r}_2,t) + H_{\rm rad}\psi_0(\boldsymbol{r}_1,\boldsymbol{r}_2)\,e^{-iE_0t}. \quad (42)$$

In the weak-field perturbative limit, which is suitable for computing single photon absorption processes, one may solve the somewhat simpler time-dependent equation given by:

$$i\frac{\partial\psi(\boldsymbol{r}_1,\boldsymbol{r}_2,t)}{\partial t} = H_{\rm atom}\psi(\boldsymbol{r}_1,\boldsymbol{r}_2,t) + H_{\rm rad}\psi_0(\boldsymbol{r}_1,\boldsymbol{r}_2)\,e^{-iE_0t}. \quad (43)$$

Upon substitution of coupled spherical harmonic expansions for both ψ and ψ_0 into equation (43), we obtain the following set of time-dependent close-coupled partial differential equations [103]:

$$i\frac{\partial P^{LS}_{l_1l_2}(r_1,r_2,t)}{\partial t} = T_{l_1l_2}(r_1,r_2)P^{LS}_{l_1l_2}(r_1,r_2,t) + \sum_{l'_1l'_2} V^{L}_{l_1l_2,l'_1l'_2}(r_1,r_2)P^{LS}_{l'_1l'_2}(r_1,r_2,t) + \sum_{l'_1l'_2} W^{LL_0}_{l_1l_2,l'_1l'_2}(r_1,r_2,t)\bar{P}^{L_0S}_{l'_1l'_2}(r_1,r_2)\,e^{-iE_0t}. \quad (44)$$

The similarities between equations (39), (44) and (3) allow very similar numerical approaches to be used in obtaining the wavefunction at some final time. An important difference is that the selection rules of the electron-photon interaction (in the dipole approximation) limit the number of L values that need to be retained in the close-coupled equations; for single photon ionization of a two-electron atom with an $L_0 = 0$ ground state, only the $L = 1$ term is required. If the initial state is not $L_0 = 0$, only two terms are required ($L = L_0 \pm 1$). The initial condition for the solution of the TDCC equations given by equation (39) is

$$P^{LS}_{l_1l_2}(r_1,r_2,t=0) = \sum_{l_1l_2}\bar{P}^{L_0S}_{l'_1l'_2}(r_1,r_2)\delta_{l_1l'_1}\delta_{l_2l'_2}\delta_{LL_0}, \quad (45)$$

and the initial condition for the solution of weak-field TDCC equations given by equation (44) is

$$P^{LS}_{l_1l_2}(r_1,r_2,t=0) = 0. \quad (46)$$

The ground-state wavefunction $\bar{P}^{L_0S}_{l_1l_2}(r_1,r_2)$ and corresponding energy E_0 are obtained by relaxation of the time-dependent Schrödinger equation (e.g. Eq. (39) with no field term present) in imaginary time. This produces the lowest eigenstate of the given symmetry on the numerical grid used. One may construct other initial states (e.g. a first excited state) by suitable orthogonalization procedures after construction of the ground state.

The projection methods used to extract scattering probabilities are very similar to those used in the electron scattering examples discussed in the previous section. We again may make use of equation (9) to obtain a momentum-space wavefunction $P^{LS}_{l_1l_2}(k_1,k_2,T)$. If one uses the weak-field version of the TDCC approach (Eq. (44)), the total double ionization cross section can be written as

$$\sigma_{\rm dion} = \frac{\omega}{I}\frac{\partial}{\partial t}\int_0^\infty dk_1\int_0^\infty dk_2\sum_{l_1l_2}|P^{LS}_{l_1l_2}(k_1,k_2,T)|^2. \quad (47)$$

The total double photoionization cross section of He and the double-to-single ionization ratio were some of the earliest sets of TDCC calculations [103], and both quantities were found to be in good agreement with measurement [106,107], as well as a range of other close-coupling calculations [15,25,108]. Total double photoionization cross sections near threshold were later examined [109] and found to be in good agreement with Wannier threshold laws.

TDCC calculations have also been presented for other two-electron atomic systems, such as H^- [110] and Li^+ in its ground and first excited states [111], as well as several other He-like ions [112]. The TDCC approach was also extended to examine other quasi two-electron systems, starting with the double photoionization of Be [113], by using similar core V_D and V_X potentials as described in Section 2.1. Total cross sections were in good agreement with convergent close-coupling calculations [28], and with later measurements [114]. TDCC calculations for the double photoionization of Li and Mg were also recently reported [115,116].

The momentum space wavefunction also allows us to define cross sections differential in energy of the outgoing electrons, using

$$\frac{d\sigma}{dE_1} = \frac{\omega}{I}\frac{\partial}{\partial t}\frac{1}{k_1 k_2}\int_0^\infty dk_1 \int_0^\infty dk_2\, \delta\left(\alpha - \tan^{-1}\frac{k_2}{k_1}\right) \times \sum_{l_1 l_2} \left|P^{LS}_{l_1 l_2}(k_1, k_2, T)\right|^2, \quad (48)$$

where E_1 is the energy of one of the outgoing electrons (with the energy of the remaining electron defined through energy conservation). The SDCS for double photoionization of He was presented in [117,118]. The usual shape of this cross section is a 'U'-shaped function, symmetric about $E/2$ (where $E = E_1 + E_2$ is the excess energy available to the outgoing electrons). The SDCS becomes flatter as the excess energy is decreased. At high photon energies [119], the SDCS becomes increasingly 'U'-shaped, with almost no probability of ejection of two equal energy electrons. This is due to the dominance of the "shake-off" mechanism in double photoionization at large photon energies.

The triple differential cross section for double photoionization of two-electron atoms can be written as

$$\frac{d^3\sigma}{dE_1 d\Omega_1 d\Omega_2} = \frac{\omega}{I}\frac{\partial}{\partial t}\frac{1}{k_1 k_2}\int_0^\infty dk_1 \int_0^\infty dk_2 \times \delta\left(\alpha - \tan^{-1}\frac{k_2}{k_1}\right) \times \sum_{l_1 l_2}\left|(-i)^{l_1+l_2}\, e^{i(\sigma_{l_1}+\sigma_{l_2})} P^{LS}_{l_1 l_2}(k_1, k_2, T)\mathcal{Y}_{l_1 l_2}(\hat{k}_1, \hat{k}_2)\right|^2, \quad (49)$$

where in this case α is the angle in the hyperspherical plane between the two outgoing momenta vectors k_1 and k_2, $\mathcal{Y}_{l_1 l_2}(\hat{k}_1, \hat{k}_2)$ is a coupled spherical harmonic, and σ_l is the Coulomb phase shift. As before, if scattering from a target with a frozen electron core is considered, one must also include the distorted-wave phase shift in equation (49). Double differential cross sections in angle may be obtained by integrating the triple differential cross section over one of the outgoing electron solid angles Ω.

The first TDCC calculations of the TDCS for double photoionization of He were presented in [117], where very good agreement with the COLTRIMS measurements of [120] was demonstrated for a range of outgoing electron angles and energies. Later, TDCC calculations [118] were also shown to be in good agreement with a variety of coincidence measurements [121–124] at various excess energies. Double and triple differential cross sections for He at high photon energies ($E = 450$ eV) [119] were also found to be in good agreement with later COLTRIMS measurements [125,126]. A selection of these TDCS calculations are presented in Figure 6 where the variation of the angular distribution as a function of the outgoing electron energy sharing is shown.

Triple differential cross sections from the $1s2s\ ^{1,3}$S states of He have also been examined [127], where more structure was observed in the TDCS compared to similar distributions from the He ground state. These structures were attributed to ionization of two electrons from different subshells. The angular distributions from double photoionization of Be [113] were also contrasted with those from He. Good agreement was observed between these angular distributions and those obtained from CCC calculations [28]. Later studies examined the effect of the increasing nuclear charge on the angular distributions from He-like ions [112]. More recently, angular distributions have also been computed for the double photoionization of Li using the TDCC method [29,30], and recoil ion distributions were found to be in good agreement with measurements [128]. The TDCC approach has also been extended to examine non-dipole contributions of the photon-electron interaction [129]. Addition of the quadrupole interaction was shown to result in only a small increase in the total double photoionization cross section, but made a significant difference to the triple differential cross sections. Dipole-only calculations had confirmed the selection rules for double photoionization predicted by Maulbetsch and Briggs [130], where back-to-back electron ejection was forbidden due to the symmetry of the outgoing electron pair. Inclusion of the quadrupole interaction however, allows back-to-back emission, since the symmetry of the ejected electron pair has changed. This effect was predicted [129] to be measurable at photon energies of 800 eV or more, although the very small cross sections make such a measurement very challenging.

3.2 Two-photon double ionization of He

For cases where more than one photon is absorbed, the "strong-field" version of the TDCC approach is suitable. If one uses the strong-field version of the TDCC approach (Eq. (39)), the total double photoionization cross section is

$$\sigma_{\rm dion} = \left(\frac{\omega}{I}\right)^n \frac{1}{T_{\rm eff}}\int_0^\infty dk_1 \int_0^\infty dk_2 \sum_{l_1 l_2} |P^{LS}_{l_1 l_2}(k_1, k_2, T)|^2, \quad (50)$$

where n is the number of photons absorbed, and $T_{\rm eff}$ is the effective pulse duration. Energy and angular differential cross sections for strong-field ionization can also be generated using analogous expressions to equations (48) and (49).

Calculations of the two-photon double ionization rates of He and H^- were presented [131] using the strong-field time-dependent close-coupling approach. These calculations were later extended [132] to compute a total cross section, as well as angular distributions at a photon energy of 45 eV. Later calculations also examined the angular distributions for a range of photon energies around 45 eV [133]. These calculations initiated a series of similar time-dependent studies, as well as a few time-independent studies, of this two-photon double ionization process using a variety of numerical approaches [38,134–145]. These

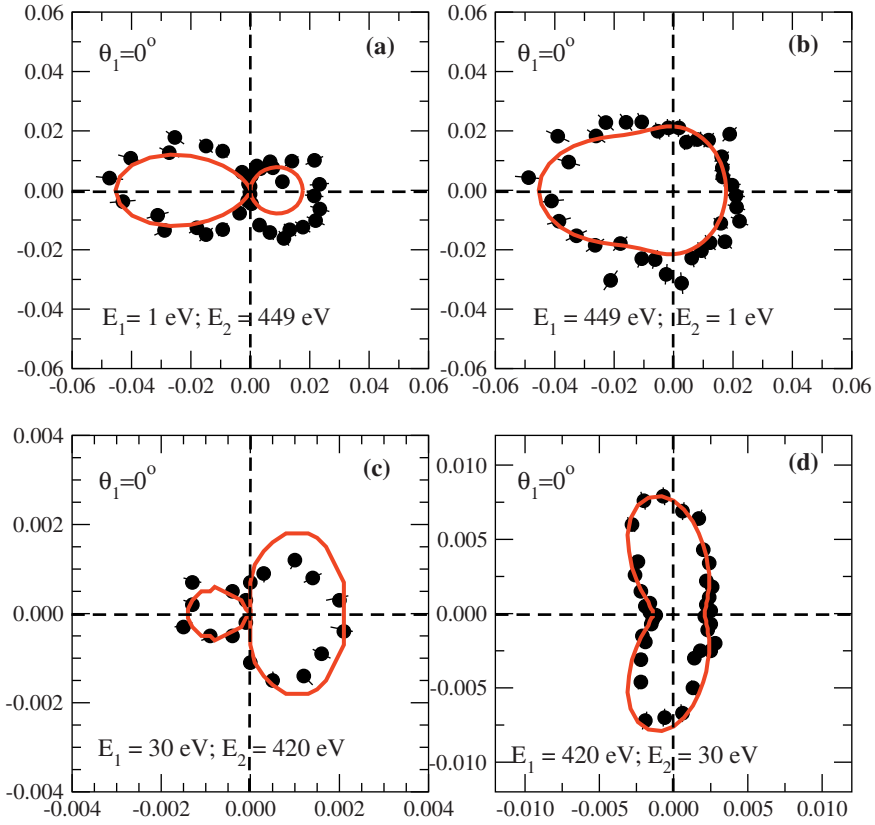

Fig. 6. Polar representation of the triple differential cross sections for He at an excess photon energy of 450 eV. The angle of the first electron is fixed at 0°. In the left two panels the fixed electron is the "slow" electron, with 1 and 30 eV energy, respectively. In the right two panels the fixed electron is the "fast" electron, with 449 and 420 eV, respectively. The TDCC calculations [119] are compared with the measurements of [125]. Cross sections are in units of b/sr^{2}eV.

further studies were motivated by some disagreements between time-dependent and time-independent calculations of the total cross section. Also, much interest has focused on the double ionization cross sections as the photon energy approaches the limit for non-sequential ionization at 54 eV. Free-electron laser (FEL) technology allows measurement of the cross sections and angular distributions for these processes [146–148], but the few existing measurements of the total cross section are not yet sufficient to fully benchmark this quantity.

3.3 Single-photon double ionization of two-electron molecules

In recent years the TDCC method has also been extended to examine double photoionization of two-electron diatomic molecules. This extension has been motivated by the impressive experimental progress in measuring the angular distributions for this double photoionization process, which has uncovered striking new physical phenomena unique to molecular break-up, such as large orientation effects [149,150], and dependence on the kinetic energy release (KER), or internuclear separation, of the molecule at the time of ionization [151,152].

We employ the formulation of the time-dependent Schrödinger equation in the weak-field perturbative limit, and write the Schrödinger equation as

$$i\frac{\partial\Psi(\boldsymbol{r}_1,\boldsymbol{r}_2,t)}{\partial t} = (H_{\rm mol}+H_{\rm rad})\Psi_0(\boldsymbol{r}_1,\boldsymbol{r}_2,t)\,e^{-iE_0t}, \quad (51)$$

where $H_{\rm mol}$ is defined by equation (14) and $H_{\rm rad}$ is again defined by equation (38) for a linearly polarized field. Substituting the rotational function expansions equation (15) into equation (51), we obtain the following set of time-dependent close-coupled partial differential equations [10]:

$$\begin{aligned} i\frac{\partial P^{MS}_{m_1m_2}(r_1,\theta_1,r_2,\theta_2,t)}{\partial t} &= T_{m_1m_2}(r_1,\theta_1,r_2,\theta_2)P^{MS}_{m_1m_2}(r_1,\theta_1,r_2,\theta_2,t) \\ &+ \sum_{m_1'm_2'} V^{M}_{m_1m_2,m_1'm_2'}(r_1,\theta_1,r_2,\theta_2)P^{MS}_{m_1'm_2'}(r_1,\theta_1,r_2,\theta_2,t) \\ &+ \sum_{m_1'm_2'} W^{MM_0}_{m_1m_2,m_1'm_2'}(r_1,\theta_1,r_2,\theta_2,t) \\ &\times \bar{P}^{M_0S}_{m_1'm_2'}(r_1,\theta_1,r_2,\theta_2)\,e^{-iE_0t}, \quad (52) \end{aligned}$$

where $T_{m_1m_2}(r_1,\theta_1,r_2,\theta_2)$ is defined by equation (17), and for linear polarization

$$W^{MM'}_{m_1m_2,m_1'm_2'}(r_1,\theta_1,r_2,\theta_2,t) = E(t)\cos\omega t\sum_{i=1}^{2} r_i\cos\theta_i\delta_{m_i,m_i'}, \quad (53)$$

while for circular polarization

$$W^{MM'}_{m_1m_2,m_1'm_2'}(r_1,\theta_1,r_2,\theta_2,t) = \frac{E(t)}{\sqrt{2}}\cos\omega t \sum_{i=1}^{2} r_i \sin\theta_i \times \int_0^{2\pi} d\phi_i \Phi_{m_i}(\phi_i)\, e^{i\phi_i}\Phi_{m_i'}(\phi_i). \quad (54)$$

The initial condition for the solution of the TDCC equations (Eq. (52)) for single photon scattering from a two-electron homonuclear diatomic molecule is given by:

$$P^{MS}_{m_1m_2}(r_1,\theta_1,r_2,\theta_2,t=0) = 0. \quad (55)$$

The expansion functions $\bar{P}^{M_0S}_{m_1m_2}(r_1,\theta_1,r_2,\theta_2)$ and energy E_0 are obtained by relaxation of the time-dependent Schrödinger equation for a two-electron molecule in imaginary time. The total double photoionization cross section for a two-electron molecule is given by:

$$\sigma_{\rm dion} = \frac{\omega}{I}\frac{\partial}{\partial t}\int_0^\infty dk_1 \int_0^\infty dk_2 \times \sum_{l_1l_2}\sum_{m_1m_2} \left|P^{MS}_{l_1m_1l_2m_2}(k_1,k_2,T)\right|^2, \quad (56)$$

where $P^{MS}_{l_1m_1l_2m_2}(k_1,k_2,T)$ is the wavefunction which results after projection of the four-dimensional radial and angular wavefunctions onto products of H_2^+ continuum states after propagation to a suitable time T, given by equation (21). Calculations of the total cross section for double photoionization of H_2 using a TDCC approach [153] were found to be in very good agreement with previous measurements [154].

Single differential cross sections for the double photoionization of a two-electron molecule can be calculated using

$$\frac{d\sigma}{dE_1} = \frac{\omega}{I}\frac{\partial}{\partial t}\frac{1}{k_1k_2}\int_0^\infty dk_1 \int_0^\infty dk_2\, \delta\left(\alpha - \tan^{-1}\frac{k_2}{k_1}\right) \times \sum_{l_1l_2}\sum_{m_1m_2} \left|P^{MS}_{l_1m_1l_2m_2}(k_1,k_2,T)\right|^2. \quad (57)$$

The triple differential cross section may be expressed as

$$\frac{d^3\sigma}{dE_1 d\Omega_1 d\Omega_2} = \frac{\omega}{I}\frac{\partial}{\partial t}\frac{1}{k_1k_2}\int_0^\infty dk_1 \int_0^\infty dk_2 \times \delta\left(\alpha - \tan^{-1}\frac{k_2}{k_1}\right)|\mathcal{M}|^2. \quad (58)$$

For diatomic molecules, where the z-axis is defined along the internuclear direction, and the polarization axis is oriented at angles (θ_k,ϕ_k) with respect to the z-axis,

$$\mathcal{M} = \sum_{M=0,\pm1} Y^*_{1M}(\theta_k,\phi_k)\sum_{l_1l_2}\sum_{m_1m_2}(-i)^{l_1+l_2}\, e^{i(\sigma_{l_1}+\sigma_{l_2})} \times P^{MS}_{l_1m_1l_2m_2}(k_1,k_2,T) Y_{l_1m_1}(\hat{k}_1) Y_{l_2m_2}(\hat{k}_2)\delta_{m_1+m_2,M}. \quad (59)$$

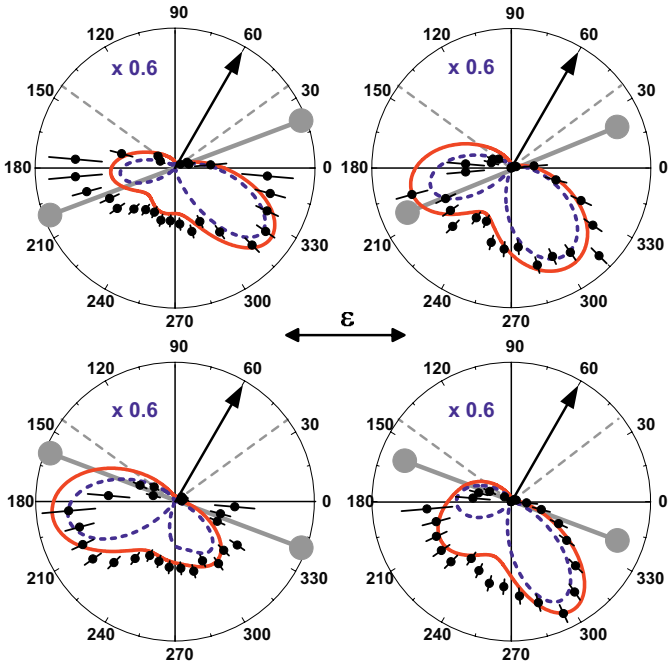

Fig. 7. Polar representation of the H_2 TDCS in the coplanar geometry for three molecular orientations as indicated [152], for fixed electron angle $\theta_1 = 60°$ and $E_1 = E_2 = 12.5 \pm 10$ eV. The left panels show measurements for a KER value of 16 eV, corresponding to an internuclear separation of $1.6\,a_0$, and the right panels show measurements for a KER value of 24 eV (internuclear separation of $1.2\,a_0$). The measurements are compared to TDCC calculations averaged over the molecular orientation uncertainties; unaveraged TDCC calculations are shown as the dashed lines.

Our TDCS expression defined by equations (58) and (59) is given in the molecular frame. As noted earlier, to compare with experiment, a transformation must be made into the Laboratory frame. The TDCS for molecular ionization is dependent on the angles between the polarization vector and the molecular axis, or equivalently, to the angle between the molecular axis and the outgoing electrons.

The first TDCC calculations of the angular distributions for double photoionization of H_2 [155] were compared to synchrotron measurements [150], and good agreement was found, after the calculations were averaged over the uncertainties in the molecular orientation angles with respect to the polarization axis. An example of such a comparison is shown in Figure 7. Calculations at exact values of molecular orientations were also found to be in excellent agreement with ECS calculations [36,156]. Later TDCC calculations [157] were also in good agreement with COLTRIMS measurements [151], and showed how the triple differential cross sections evolve as the number of field periods increases. More recently, TDCC calculations at different internuclear separations were able to shed some light on the "KER" effect in double photoionization of H_2 [152], where it was found that interference between the contributing Σ ($M = 0$) and Π ($M = \pm1$) amplitudes gives rise to the strong dependence of the electron angular distributions on the kinetic energy of the

outgoing protons that result after Coulomb explosion of the molecule after double ionization. The TDCC approach has also been used to uncover new fragmentation patterns in the double photoionization of H_2 [158] which were predicted by a novel characterization of the outgoing electron pair. Very recently, an alternative TDCC formulation in prolate spherical coordinates [159] has also been proposed, and applied to the same process of double photoionization of H_2. Finally, we also mention that recently several two-photon double ionization TDCC calculations of H_2 have been reported [160–162]. Such calculations have proven difficult to converge, and the effects of the pulse shape and length, as well as the influence of double excited states of H_2, are found to significantly influence the resulting cross sections.

3.4 Single-photon triple ionization of three-electron atoms

The TDCC approach has been applied to *triple* photoionization, that is, ionization of all three electrons by absorption of a single photon. As in the electron-impact double ionization of two-electron systems, the extension to three active electrons results in a significantly more complicated calculation, as well as a very computationally intensive problem.

The time-dependent Schrödinger equation for a three-electron atom in a weak time-varying electromagnetic field is given by:

$$i\frac{\partial\psi(\boldsymbol{r}_1,\boldsymbol{r}_2,\boldsymbol{r}_3,t)}{\partial t} = H_{\rm atom}\psi(\boldsymbol{r}_1,\boldsymbol{r}_2,\boldsymbol{r}_3,t) + H_{\rm rad}\psi_0(\boldsymbol{r}_1,\boldsymbol{r}_2,\boldsymbol{r}_3)\,e^{-iE_0t} \quad (60)$$

where the non-relativistic Hamiltonian for the atom is given by equation (26) and the Hamiltonian for a linearly polarized radiation field is given by:

$$H_{\rm rad} = E(t)\cos\omega t\sum_{i=1}^{3} r_i\cos\theta_i. \quad (61)$$

Upon substitution of coupled spherical harmonic expansions equation (27) for both ψ and ψ_0 into equation (60), we obtain the following set of time-dependent close-coupled partial differential equations [10]:

$$\begin{aligned} i\frac{\partial P^{\mathcal{LS}}_{l_1l_2Ll_3}(r_1,r_2,r_3,t)}{\partial t} &= T_{l_1l_2l_3}(r_1,r_2,r_3)P^{\mathcal{LS}}_{l_1l_2Ll_3}(r_1,r_2,r_3,t) \\ &+ \sum_{l_1'l_2'L'l_3'}\sum_{i<j=1}^{3} V^{\mathcal{L}}_{l_1l_2Ll_3,l_1'l_2'L'l_3'}(r_i,r_j)P^{\mathcal{LS}}_{l_1'l_2'L'l_3'}(r_1,r_2,r_3,t), \\ &+ \sum_{l_1'l_2'L'l_3'}\sum_{i=1}^{3} W^{\mathcal{LL}_0}_{l_1l_2Ll_3,l_1'l_2'L'l_3'}(r_i,t)\bar{P}^{\mathcal{L}_0\mathcal{S}}_{l_1'l_2'L'l_3'}(r_1,r_2,r_3)e^{-iE_0t}, \end{aligned} \quad (62)$$

where $V^{\mathcal{L}}_{l_1l_2Ll_3,l_1'l_2'L'l_3'}(r_i,r_j)$ are two-electron coupling operators, and $W^{\mathcal{LL}_0}_{l_1l_2Ll_3,l_1'l_2'L'l_3'}(r_i,t)$ represents the coupling of each electron to the electromagnetic field. The initial condition for these equations is as before

$$P^{\mathcal{LS}}_{l_1l_2Ll_3}(r_1,r_2,r_3,t=0) = 0. \quad (63)$$

The expansion functions $\bar{P}^{\mathcal{L}_0\mathcal{S}}_{l_1l_2Ll_3}(r_1,r_2,r_3)$ and energy E_0 are obtained by relaxation of the time-dependent Schrödinger equation for a three-electron atom in imaginary time. For the Li ground state, orthogonalization procedures are necessary to prevent the unphysical relaxation to a $1s^3$ eigenstate.

The total cross section for triple ionization can be expressed as

$$\sigma_{\rm tion} = \frac{\omega}{I}\frac{\partial}{\partial t}\int_0^\infty dk_1\int_0^\infty dk_2\int_0^\infty dk_3 \times\sum_{l_1l_2LSl_3}\left|P^{\mathcal{LS}}_{l_1l_2Ll_3}(k_1,k_2,k_3,T)\right|^2, \quad (64)$$

where $P^{\mathcal{LS}}_{l_1l_2Ll_3}(k_1,k_2,k_3,T)$ is again a three-electron momentum-space wavefunction obtained by projection of the coordinate space wavefunction at a final time T following equations (31) and (32). The first TDCC calculations explored the total cross section for the triple photoionization of Li [163], where good agreement was found with the only existing synchrotron measurements [164]. The total cross sections for Li were later extended, and triple photoionization cross sections were also presented for Be [165].

As in the two-electron case, one may obtain energy and angular differential cross sections for the triple photoionization process. The double energy differential cross section can be written as:

$$\begin{aligned} \frac{d^2\sigma}{dE_2dE_3} = \frac{\omega}{I}\frac{\partial}{\partial t}&\frac{1}{k_1k_2k_3\sqrt{k_1^2+k_2^2}} \\ &\times\int_0^\infty dk_1\int_0^\infty dk_2\int_0^\infty dk_3 \\ &\times\delta\left(\alpha-\tan^{-1}\frac{k_2}{k_1}\right)\delta\left(\beta-\tan^{-1}\frac{k_3}{\sqrt{k_1^2+k_2^2}}\right) \\ &\times\sum_{l_1l_2l_3LS}\frac{1}{6}\sum_{ijk}^{6}\left|P^{\mathcal{LS}}_{l_1l_2LSl_3}(k_i,k_j,k_k,T)\right|^2, \end{aligned} \quad (65)$$

where α is an angle in the (k_1,k_2) hyperspherical plane and β is an angle in the plane perpendicular to the (k_1,k_2) hyperspherical plane, both defined from 0 to $\frac{\pi}{2}$. The energy differential cross sections for triple photoionization of Li were previously presented [166], and "cuts" through the double energy differential distributions were found to be qualitatively similar to the single energy differential distributions found in the double photoionization of He.

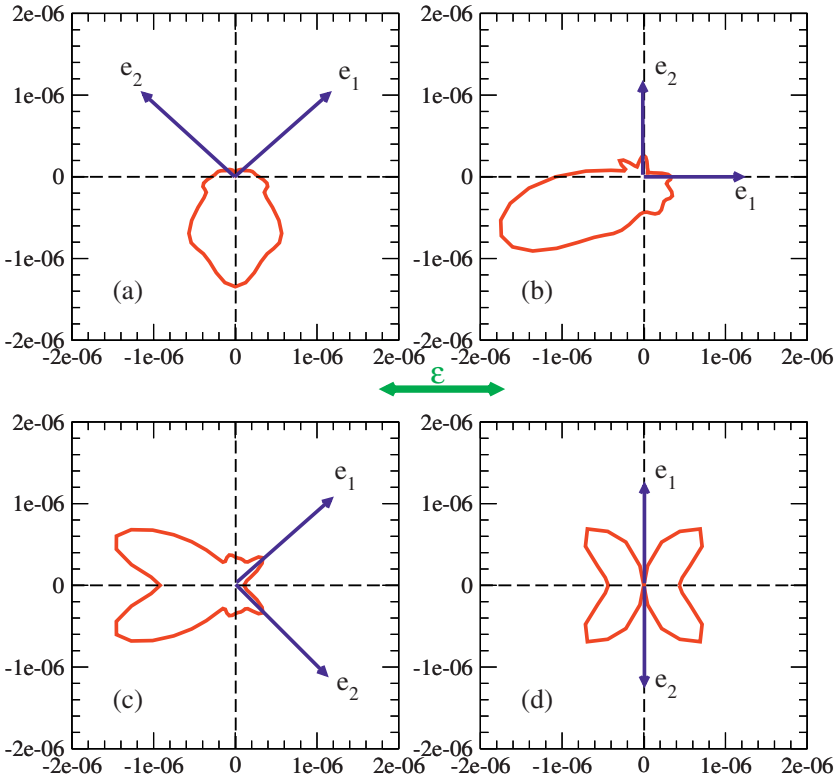

Fig. 8. Polar representation of the pentuple differential cross sections for triple photoionization of Li at a photon energy of 300 eV and for $E_1 = E_2 = E_3 = 33$ eV [167]. Results are presented as a function of θ_3 for fixed values of θ_1 and θ_2. (a) $\theta_1 = 45°$, $\theta_2 = 135°$; (b) $\theta_1 = 0°$, $\theta_2 = 90°$; (c) $\theta_1 = 45°$, $\theta_2 = 315°$; (d) $\theta_1 = 90°$, $\theta_2 = 270°$. All cross sections are in units of b/(sr^3 eV^2).

The pentuple energy and angle differential cross section for triple photoionization is given by:

$$\frac{d^5\sigma}{dE_2 dE_3 d\Omega_1 d\Omega_2 d\Omega_3} = \frac{\omega}{I}\frac{\partial}{\partial t}\frac{1}{k_1 k_2 k_3\sqrt{k_1^2+k_2^2}} \times \int_0^\infty dk_1 \int_0^\infty dk_2 \int_0^\infty dk_3 \times \delta\left(\alpha - \tan^{-1}\frac{k_2}{k_1}\right)\delta\left(\beta - \tan^{-1}\frac{k_3}{\sqrt{k_1^2+k_2^2}}\right) \times \sum_S \frac{1}{6}\sum_{ijk}^{6}\left|\sum_{l_1 l_2 l_3 L}(-i)^{l_1+l_2+l_3} e^{i(\sigma_{l_1}(k_i)+\sigma_{l_2}(k_j)+\sigma_{l_3}(k_k))} \times P^{\mathcal{LS}}_{l_1 l_2 L S l_3}(k_i,k_j,k_k,T)\mathcal{Y}_{l_1 l_2 L l_3 \mathcal{L}}(\Omega_i,\Omega_j,\Omega_k)\right|^2, \quad (66)$$

where σ_l is a Coulomb phase shift and $\mathcal{Y}_{l_1 l_2 L l_3 \mathcal{L}}$ is a coupled product of three spherical harmonics. The integrals over linear momenta are again restricted so that the total energy (Eq. (33)) is approximately conserved. A variety of angular distributions for triple photoionization of Li were recently presented [167] and the dominant fragmentation channels discussed. An example of the angular distributions for four equal energy sharing cases is shown in Figure 8.

4 Ion-impact ionization of small atoms and molecules

4.1 Ion-impact ionization of small atoms

The time-dependent close-coupling method was first applied to examine the double ionization of He by fast bare ion projectiles [168]. The approach is suitable for high incident projectile energies, where charge exchange may be neglected. The Schrödinger equation for the ionization of a two-electron atom by a fast bare ion is written as

$$i\frac{\partial\Psi(\boldsymbol{r}_1,\boldsymbol{r}_2,t)}{\partial t} = (H_{\rm atom} + H_{\rm proj})\Psi(\boldsymbol{r}_1,\boldsymbol{r}_2,t), \quad (67)$$

where the non-relativistic Hamiltonian for the atom is given by equation (2) and the Hamiltonian representing the interaction of the fast ion (of charge Z_p) with the two electrons is given by

$$H_{\rm proj} = -\frac{Z_p}{|\boldsymbol{r}_1 - \boldsymbol{R}(t)|} - \frac{Z_p}{|\boldsymbol{r}_2 - \boldsymbol{R}(t)|}. \quad (68)$$

For straight-line motion, the magnitude of the time-dependent projectile position is given by:

$$R(t) = \sqrt{b^2 + (d_0 + vt)^2}, \quad (69)$$

where b is an impact parameter, d_0 is a starting distance ($d_0 < 0$), and v is the projectile speed. By again expanding

the total wavefunction for the two electrons in coupled spherical harmonics we obtain the following set of close-coupled partial differential equations

$$i\frac{\partial P^{LMS}_{l_1l_2}(r_1,r_2,t)}{\partial t} = T_{l_1l_2}(r_1,r_2)P^{LMS}_{l_1l_2}(r_1,r_2,t) + \sum_{l_1'l_2'} V^{L}_{l_1l_2,l_1'l_2'}(r_1,r_2)P^{LMS}_{l_1'l_2'}(r_1,r_2,t) + \sum_{l_1'l_2'} W^{LM,L'M'}_{l_1l_2,l_1'l_2'}(r_1,R(t))P^{L'M'S'}_{l_1'l_2'}(r_1,r_2,t) + \sum_{l_1'l_2'} W^{LM,L'M'}_{l_1l_2,l_1'l_2'}(r_2,R(t))P^{L'M'S'}_{l_1'l_2'}(r_1,r_2,t), \quad (70)$$

where $V^{L}_{l_1l_2,l_1'l_2'}(r_1,r_2)$ is defined by equation (5),

$$W^{LM,L'M'}_{l_1l_2,l_1'l_2'}(r_1,R(t)) = -Z_p\delta_{l_2,l_2'}(-1)^{l_2+L+L'-M} \times \sqrt{(2l_1+1)(2l_1'+1)(2L+1)(2L'+1)} \times \sum_{\lambda}(-1)^{\lambda}\frac{(r_1,R(t))^{\lambda}_{<}}{(r_1,R(t))^{\lambda+1}_{>}}\begin{pmatrix} l_1 & \lambda & l_1' \\ 0 & 0 & 0\end{pmatrix} \times \sum_{q} C^{\lambda *}_{q}(\theta,\phi)\begin{pmatrix} L & \lambda & L' \\ -M & q & M'\end{pmatrix}\begin{Bmatrix} l_1 & l_2 & L \\ L' & \lambda & l_1'\end{Bmatrix}, \quad (71)$$

and

$$W^{LM,L'M'}_{l_1l_2,l_1'l_2'}(r_2,R(t)) = -Z_p\delta_{l_1,l_1'}(-1)^{l_1+l_2+l_2'-M} \times \sqrt{(2l_2+1)(2l_2'+1)(2L+1)(2L'+1)} \times \sum_{\lambda}(-1)^{\lambda}\frac{(r_2,R(t))^{\lambda}_{<}}{(r_2,R(t))^{\lambda+1}_{>}}\begin{pmatrix} l_2 & \lambda & l_2' \\ 0 & 0 & 0\end{pmatrix} \times \sum_{q} C^{\lambda *}_{q}(\theta,\phi)\begin{pmatrix} L & \lambda & L' \\ -M & q & M'\end{pmatrix}\begin{Bmatrix} l_1 & l_2 & L \\ \lambda & L' & l_2'\end{Bmatrix}. \quad (72)$$

The spherical tensor in equations (71) and (72) is defined by:

$$C^{\lambda}_{q}(\theta,\phi) = \sqrt{\frac{4\pi}{2\lambda+1}}Y^{\lambda}_{q}(\theta,\phi), \quad (73)$$

where $Y^{\lambda}_{q}(\theta,\phi)$ is a spherical harmomic. Each λ term in equations (71) and (72) corresponds to a contribution from the multipole interaction between the fast ion and each electron. We find that expansions to at least the octopole term ($\lambda \leq 3$) are required to fully converge the resulting ionization cross sections.

The initial condition for the solution of the time-dependent equations (70) is

$$P^{LMS}_{l_1l_2}(r_1,r_2,t=0) = \delta_{L,L_0}\delta_{M,M_0}\bar{P}^{L_0M_0S_0}_{l_1l_2}(r_1,r_2), \quad (74)$$

where $\bar{P}^{L_0M_0S_0}_{l_1l_2}(r_1,r_2)$ is the ground-state wavefunction for the two-electron atom, obtained by relaxation of the time-dependent Schrödinger equation in imaginary time, in the same manner as described in the photon-atom interaction discussed in Section 3.

To obtain ionization probabilities and cross sections, we may use projection methods that are very similar to those described in the previous sections. We employ an expression similar to equation (9) to obtain a momentum-space wavefunction $P^{LMS}_{l_1l_2}(k_1,k_2,b,T)$ at some final time T, except that now we must remove the overlap with the initial ground state. The momentum space wavefunctions are thus given by

$$P^{LMS}_{l_1l_2}(k_1,k_2,b,T) = \int_0^{\infty} dr_1 \int_0^{\infty} dr_2 \times P_{k_1l_1}(r_1)P_{k_2l_2}(r_2)\hat{P}^{LMS}_{l_1l_2}(r_1,r_2,t=T), \quad (75)$$

where $\hat{P}^{LMS}_{l_1l_2}(r_1,r_2,t=T)$ is given by

$$\hat{P}^{LMS}_{l_1l_2}(r_1,r_2,t=T) = P^{LMS}_{l_1l_2}(r_1,r_2,t=T) - \beta\bar{P}^{L_0M_0S_0}_{l_1l_2}(r_1,r_2)\delta_{L,L_0}\delta_{M,M_0}\delta_{S,S_0}, \quad (76)$$

and β is the overlap of the initial state with the final state, defined as

$$\beta = \sum_{l_1l_2}\int_0^{\infty} dr_1 \int_0^{\infty} dr_2 \bar{P}^{L_0M_0S_0}_{l_1l_2}(r_1,r_2) \times P^{L_0M_0S_0}_{l_1l_2}(r_1,r_2,t=T). \quad (77)$$

The probability for double ionization at a given impact parameter is then given by

$$\mathcal{P}_{\rm dion}(v,b) = \int_0^{\infty} dk_1 \int_0^{\infty} dk_2 \times \sum_{l_1,l_2,L,M}\left|P^{LMS}_{l_1l_2}(k_1,k_2,b,T)\right|^2. \quad (78)$$

The calculation proceeds by repeatedly solving the TDCC equations for all impact parameters b until the contribution to the ionization probability from large b values becomes small. The total double ionization cross section can then be written as

$$\sigma_{\rm dion}(v) = 2\pi\int_0^{\infty}\mathcal{P}_{\rm dion}(v,b)\, bdb. \quad (79)$$

One may also obtain single ionization cross sections by computing the single ionization probability given by

$$\mathcal{P}_{\rm sion}(v,b) = \sum_{nl}\int_0^{\infty} dk \sum_{l_1l_2LM}\left|P^{LMS}_{l_1l_2}(nl,k,b,T)\right|^2, \quad (80)$$

where

$$P_{l_1 l_2}^{LMS}(nl,k,b,T) = \Bigg(\Bigg| \int_0^\infty dr_1 \int_0^\infty dr_2 P_{nl_1}(r_1) P_{kl_2}(r_2) \times \hat{P}_{l_1 l_2}^{LMS}(r_1,r_2,t=T)\delta_{l,l_1} \Bigg|^2 + \Bigg| \int_0^\infty dr_1 \int_0^\infty dr_2 P_{kl_1}(r_1) P_{nl_2}(r_2) \times \hat{P}_{l_1 l_2}^{LMS}(r_1,r_2,t=T)\delta_{l,l_2} \Bigg|^2 \Bigg). \quad (81)$$

The resulting total single ionization cross section then given by

$$\sigma_{\rm sion}(v) = 2\pi \frac{w_t}{l_t+1} \int_0^\infty \mathcal{P}_{\rm sion}(v,b)\, b db, \quad (82)$$

where w_t is the occupation number of the initial subshell with angular momentum l_t. The first TDCC ion-impact calculations were of total cross sections for single and double ionization of He by fast α particles [168], and good agreement was found between the time-dependent calculations and measurement [169]. Subsequently, single and double ionization of He by antiproton ($\bar{p}$) impact was also investigated [170]. Antiproton impact calculations are particularly attractive since there is no possibility of charge exchange, and so calculations may be performed for a wide range of incident projectile energies. Good agreement was found between the TDCC single ionization calculations and measurements [171,172], except at the lowest impact energies considered. For double ionization, good agreement between the TDCC double ionization calculations and measurement [171] was found for almost all incident energies, and a later, separate TDCC calculation also demonstrated similar agreement [173]. A more recent measurement [174] at low energies was also consistent with the TDCC calculations. It was also found [170] that the double ionization of He by $\bar{p}$-impact was twice as large as proton impact double ionization at a given incident energy, even though the single ionization cross sections from both projectiles are quite similar. This finding is presented in Figure 9 [170].

More recently, total single ionization cross sections for $\bar{p}$ impact of H, He, and Li at low impact energies have been presented [175]. A single-active-electron time-dependent approach was used, as well as the full two-electron TDCC approach described here. The single-active-electron approach was found to be in good agreement with total cross section measurements for H and Li, but considerably higher than measurement and two-electron TDCC calculations for He. As the incident energy increases, the single-active-electron and two-electron time-dependent calculations are in much better agreement.

One may also compute a variety of differential cross sections arising from ion-impact single and double ionization. The double differential (in angles of the outgoing electrons) cross section for proton-impact double

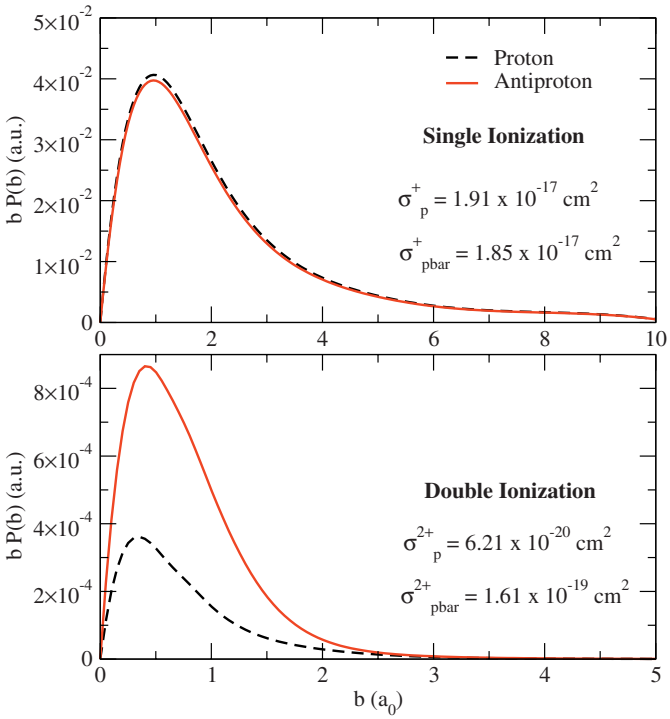

Fig. 9. Weighted probabilities for single (upper) and double (lower) ionization of He by antiproton (red line) and proton (black dashed line) impact at 1 MeV impact energy [170].

ionization of helium can be written as

$$\frac{d^2\sigma}{d\Omega_1 d\Omega_2} = \int_0^\infty dk_1 \int_0^\infty dk_2 \int_0^\infty 2\pi\, db\, b \times \Bigg| \sum_{l_1 l_2 LM} (-i)^{l_1+l_2}\, e^{i(\sigma_{l_1}+\sigma_{l_2})} \times P_{l_1 l_2}^{LMS}(k_1,k_2,b,T) \mathcal{Y}_{l_1 l_2}^{LM}(\hat{k}_1,\hat{k}_2) \Bigg|^2, \quad (83)$$

where σ_l is again the Coulomb phase shift, $\mathcal{Y}_{l_1 l_2}^{LM}(\hat{k}_1,\hat{k}_2)$ are coupled spherical harmonics, and integration over all solid angles and impact parameters b, recovers the total double ionization cross section. It is straightforward to compute further cross sections that are also differential in the energy shared between the outgoing electrons, following the approach used in Section 3. Double ionization of He by proton impact at 6 MeV incident energy was recently reported [173,176,177], where reasonable agreement was found between the TDCC calculations and the only measurements available [178].

Differential cross sections may also be computed for single ionization by ion impact within the two-electron TDCC approach [179]. One may construct a function that depends on the angles of the ejected electron by using the single-ionization momentum-space wavefunction defined by equation (81). For single ionization leaving the

$$i\frac{\partial P^{MS}_{m_1m_2}(r_1,\theta_1,r_2,\theta_2,t)}{\partial t} = T_{m_1m_2}(r_1,\theta_1,r_2,\theta_2)P^{MS}_{m_1m_2}(r_1,\theta_1,r_2,\theta_2,t) + \sum_{m_1'm_2'} V^{M}_{m_1m_2,m_1'm_2'}(r_1,\theta_1,r_2,\theta_2)P^{MS}_{m_1'm_2'}(r_1,\theta_1,r_2,\theta_2,t) + \sum_{m_1'm_2'M'} W^{MM'}_{m_1m_2,m_1'm_2'}(r_1,\theta_1,R_p,\theta_p,t)P^{M'S}_{m_1',m_2'}(r_1,\theta_1,r_2,\theta_2,t) + \sum_{m_1'm_2'M'} W^{MM'}_{m_1m_2,m_1'm_2'}(r_2,\theta_2,R_p,\theta_p,t)P^{M'S}_{m_1',m_2'}(r_1,\theta_1,r_2,\theta_2,t), \quad (88)$$

ion in a $1s$ state, this function takes the form

$$P(\hat{k},b) = \sum_{LM}(-i)^L\, e^{i\sigma_L} P^{LMS}_{0L}(1s,k,b,T)Y_{LM}(\hat{k}), \quad (84)$$

where $P^{LMS}_{0L}(1s,k,b,T)$ is defined by equation (81) with $nl \equiv 1s$. A (fully) differential cross section, differential in also the projectile scattering angle (or, equivalently in the momentum transfer η of the projectile) may then be computed using [180]

$$P(\hat{k},\eta) = \frac{1}{2\pi}\sum_{n=-\infty}^{n=+\infty} i^n \int_0^{2\pi} d\phi_b\, e^{-in\phi_b} \times \int b\, dbP(\hat{k},b)\, e^{i\delta(b)} J_n(\eta b), \quad (85)$$

where J_n is a Bessel function of order n. The fully differential cross section is then given by

$$\frac{d^4\sigma}{d\theta_e d\phi_e dk d\eta} = 2|P(\hat{k},\eta)|^2. \quad (86)$$

We have recently examined the single ionization of He by fast C^{6+} ions at 100 MeV/amu energy. This study was prompted by ongoing discrepancies between a measurement of the fully differential cross section in the plane perpendicular to the projectile direction and momentum transfer [181], and perturbative calculations. A perturbative approach had been expected to be quite valid at such high incident energies, and also showed good agreement with measurements in the scattering plane. Our TDCC calculations for single ionization [179,180] were also in good agreement with measurement in the scattering plane. In the perpendicular plane, TDCC calculations found similar structures (a double-peak distribution) to the experimental fully differential cross sections, although the magnitude of the calculations were much lower than the measurements. However, the shape of our TDCC calculations disagreed with the "flat" distribution predicted from perturbative calculations [181] and more recent pseudo-state calculations [182].

4.2 Ion-impact ionization of small molecules

The time-dependent close-coupling method was first applied to examine the double ionization of H_2 by fast bare ion projectiles [183]. The Schrödinger equation for the ionization of a two-electron diatomic molecule by a fast bare ion is written as

$$i\frac{\partial\Psi(\boldsymbol{r}_1,\boldsymbol{r}_2,t)}{\partial t} = (H_{\rm mol} + H_{\rm proj})\Psi(\boldsymbol{r}_1,\boldsymbol{r}_2,t), \quad (87)$$

where the non-relativistic Hamiltonian for the molecule is given by equation (14) and the projectile Hamiltonian is given by equation (68). By expanding the six-dimensional target wavefunction in rotation functions equation (15), and substitution into the time-dependent Schrödinger equation, we obtain

see equation (88) above,

where $T_{m_1m_2}(r_1,\theta_1,r_2,\theta_2)$ is defined by equation (17), $V^{M}_{m_1m_2,m_1'm_2'}(r_1,\theta_1,r_2,\theta_2)$ is defined by equation (18), and the electron projectile operators are defined by [183] as

$$W^{MM'}_{m_1m_2,m_1'm_2'}(r_1,\theta_1,R_p,\theta_p,t) = -Z_p\delta_{m_2,m_2'} \times \sum_{\lambda=0}^{\lambda_{max}} \frac{(r_1,R_p)^{\lambda}_{<}}{(r_1,R_p)^{\lambda+1}_{>}} \sum_{q=-\lambda}^{+\lambda} C^{\lambda *}_q(\theta_p,\phi_p)Y_{\lambda q}(\theta_1,0) \times \sqrt{\frac{4\pi}{2\lambda+1}}\delta_{q,m_1-m_1'} \quad (89)$$

and

$$W^{MM'}_{m_1m_2,m_1'm_2'}(r_2,\theta_2,R_p,\theta_p,t) = -Z_p\delta_{m_1,m_1'} \times \sum_{\lambda=0}^{\lambda_{max}} \frac{(r_2,R_p)^{\lambda}_{<}}{(r_2,R_p)^{\lambda+1}_{>}} \sum_{q=-\lambda}^{+\lambda} C^{\lambda *}_q(\theta_p,\phi_p)Y_{\lambda q}(\theta_2,0) \times \sqrt{\frac{4\pi}{2\lambda+1}}\delta_{q,m_2-m_2'}. \quad (90)$$

The z-axis is chosen to be along the internuclear axis of the molecule, and (θ_p,ϕ_p) are the angles made by the projectile with respect to this z-axis. In principle, one must perform calculations for all possible projectile directions relative to the internuclear axis. Fortunately, it has been found [184,185] that consideration of just three orientations (projectile motion along the x, y, and z-axes) is often sufficient to recover the total cross section for ion-impact ionization of an arbitrarily aligned molecule. This approximation improves quickly with increasing projectile energy.

$$P^{MS}_{l_1m_1l_2m_2}(nl,k,b,T) = \Bigg(\Bigg| \int_0^\infty dr_1 \int_0^\pi d\theta_1 \int_0^\infty dr_2 \int_0^\pi d\theta_2 \; P_{nl_1|m_1|}(r_1,\theta_1) P_{kl_2|m_2|}(r_2,\theta_2) \times \hat{P}^{MS}_{m_1m_2}(r_1,\theta_1,r_2,\theta_2,t=T)\delta_{l,l_1}\delta_{m,m_1}\Bigg|^2 + \Bigg| \int_0^\infty dr_1 \int_0^\pi d\theta_1 \int_0^\infty dr_2 \int_0^\pi d\theta_2 P_{kl_1|m_1|}(r_1,\theta_1) P_{nl_2|m_2|}(r_2,\theta_2) \times \hat{P}^{MS}_{m_1m_2}(r_1,\theta_1,r_2,\theta_2,t=T)\delta_{l,l_2}\delta_{m,m_2}\Bigg|^2\Bigg). \quad (93)$$

The initial condition for the solution of equation (88) is given by

$$P^{MS}_{m_1m_2}(r_1,\theta_1,r_2,\theta_2,t=0) = \bar{P}^{M_0S}_{m_1m_2}(r_1,\theta_1,r_2,\theta_2), \quad (91)$$

where the expansion functions $\bar{P}^{M_0S}_{m_1m_2}(r_1,\theta_1,r_2,\theta_2)$ are again obtained by relaxation of the time-dependent Schrödinger equation, with no electron-projectile interaction terms, for a two-electron molecule in imaginary time.

Probabilities for single ionization of the two-electron molecule can be written as

$$\mathcal{P}_{\rm sion}(v,b) = \sum_{nl}\int_0^\infty dk \sum_{l_1l_2}\sum_{m_1m_2M} \times \left|P^{MS}_{l_1m_1l_2m_2}(nl,k,b,T)\right|^2, \quad (92)$$

where

see equation (93) above.

The probability for double ionization can be expressed as

$$\mathcal{P}_{\rm dion}(v,b) = \int_0^\infty dk_1 \int_0^\infty dk_2 \times \sum_{l_1l_2}\sum_{m_1m_2M}\left|P^{MS}_{l_1m_1l_2m_2}(k_1,k_2,b,T)\right|^2. \quad (94)$$

The momentum-space wavefunctions $P^{MS}_{l_1m_1l_2m_2}(k_1,k_2,b,T)$ are similar to equation (21), but as in the ion-atom case, we must remove the overlap with the initial ground state, so that we employ the expression

$$P^{MS}_{l_1m_1l_2m_2}(k_1,k_2,b,T) = \int_0^\infty dr_1 \int_0^\pi d\theta_1 \int_0^\infty dr_2 \int_0^\pi d\theta_2 \times P_{k_1l_1|m_1|}(r_1,\theta_1) P_{k_2l_2|m_2|}(r_2,\theta_2) \times \hat{P}^{MS}_{m_1m_2}(r_1,\theta_1,r_2,\theta_2,t=T), \quad (95)$$

where $\hat{P}^{MS}_{m_1m_2}(r_1,\theta_1,r_2,\theta_2,t=T)$ is given by

$$\hat{P}^{MS}_{m_1m_2}(r_1,\theta_1,r_2,\theta_2,t=T) = P^{MS}_{m_1m_2}(r_1,\theta_1,r_2,\theta_2,t=T) - \beta\bar{P}^{M_0S_0}_{m_1m_2}(r_1,\theta_1,r_2,\theta_2)\delta_{M,M_0}\delta_{S,S_0}, \quad (96)$$

and β is again the overlap of the initial state with the final state, defined as

$$\beta = \sum_{m_1m_2}\int_0^\infty dr_1 \int_0^\pi d\theta_1 \int_0^\infty dr_2 \int_0^\pi d\theta_2 \times \bar{P}^{M_0S_0}_{m_1m_2}(r_1,\theta_1,r_2,\theta_2) P^{M_0S_0}_{m_1m_2}(r_1,\theta_1,r_2,\theta_2,t=T). \quad (97)$$

The total cross sections for single and double ionization are then given by equations (82) and (79), respectively.

The ratio of double-to-single ionization for proton impact of H_2 at 1 MeV was reported to be 0.3% [183], in reasonable agreement with measurement [186]. Further time-dependent calculations [185,187] examined the antiproton-impact single and double ionization of H_2. Single ionization cross section calculations were found to be in reasonable agreement with measurement [171,188]. The molecular momentum-space wavefunctions also can be used to compute a variety of differential cross sections for ion-impact ionization of molecules, although such computationally intensive calculations await further supercomputing resources and supporting measurements.

5 Conclusions

In this colloquium we have reviewed recent progress on the application of the time-dependent close-coupling approach to electron, photon and ion impact ionization of small atoms and molecules. A time-dependent approach is found to be most useful in such problems, which often involve two or more charged particles moving in a Coulomb field of an atomic or molecular ion. This is because, unlike most time-independent approaches, a boundary condition is not required to obtain scattering information. We have shown how the application of the TDCC approach produces accurate scattering cross sections for most collision systems studied so far, and also can provide insight into the underlying physics of the scattering process. Notable recent examples in this regard include the exploration of the kinetic energy release effect in the double photoionization of H_2, and the analysis of the deep minimum found in the triple differential cross sections for electron-impact ionization of He.

There are many research areas in which future application of the TDCC approach may prove beneficial. A prominent example concerns systems in which the interaction between the outgoing electrons and core electrons

is important and cannot easily be described by a model or pseudo potential, such as found in the double photoionization of Ne. In such cases, accurate treatment of the interaction between the core electrons and the outgoing electrons is required, as well as an accurate treatment of the interaction between the outgoing electrons, to obtain accurate scattering information.

A second future research avenue may involve extension of the three-active-electron TDCC approach (as discussed here for triple photoionization of Li and electron-impact double ionization of He) to molecular systems. Such an approach is required to properly model the electron-impact ionization-excitation and/or double ionization of H_2. A few measurements of such processes have been reported and future studies are planned. Although the extension of a three-electron TDCC approach to four-active-electrons may also seem natural, we do not envision such an extension in the near future. Such calculations would of course be formidably complex, but more importantly few (if any) current or planned measurements explore problems in which four electrons strongly interact in the continuum.

We are grateful for long-standing collaborations with many researchers in the atomic collision field over the years, and in particular wish to thank F. Robicheaux, D.C. Griffin, C.P. Ballance, S.D. Loch, D. Schultz, G.S.J. Armstrong, C.J. Fontes, J.C. Berengut, T. Topcu, M. Foster, T. Minami, N.R. Badnell, M.C. Witthoeft, D.R. Plante, D.M. Mitnik, J.A. Ludlow, U. Kleiman, T.G. Lee, and Sh.A. Abdel-Naby. The Los Alamos National Laboratory is operated by Los Alamos National Security, LLC for the NNSA of the U.S. DOE under Contract No. DE-AC5206NA25396. Much of the work described here was supported in part by grants from the U.S. DOE and from the U.S. NSF to Auburn University. Computational work was carried out at the NERSC in Oakland, California, the NICS in Knoxville, Tennessee, and at Los Alamos National Laboratory.

References

1. M.R.H. Rudge, M.J. Seaton, Proc. Roy. Soc. **283**, 262 (1965)
2. R. Peterkop, J. Phys. B **4**, 513 (1971)
3. C. Bottcher, J. Phys. B **15**, L463 (1982)
4. C. Bottcher, Adv. At. Mol. Phys. **20**, 241 (1985)
5. M.S. Pindzola, D.R. Schultz, Phys. Rev. A **53**, 1525 (1996)
6. M.S. Pindzola, F. Robicheaux, Phys. Rev. A **54**, 2142 (1996)
7. W. Ihra, M. Draeger, G. Handke, H. Friedrich, Phys. Rev. A **52**, 3752 (1995)
8. F. Robicheaux, M.S. Pindzola, D.R. Plante, Phys. Rev. A **55**, 3573 (1997)
9. M.S. Pindzola, F. Robicheaux, Phys. Rev. A **55**, 4617 (1997)
10. M.S. Pindzola et al., J. Phys. B **40**, R39 (2007)
11. R. Dörner, V. Mergel, O. Jagutzki, L. Spielberger, J. Ullrich, R. Moshammer, H. Schmidt-Böcking, Phys. Rep. **330**, 95 (2000)
12. *Atomic and Molecular Processes: an R-matrix approach*, edited by P.G. Burke, K.A. Berrington (Bristol Institute of Physics Publishing, 1993)
13. P.G. Burke, *R-Matrix Theory of Atomic Collisions: Application to Atomic, Molecular and Optical Processes* (Springer-Verlag, Berlin, 2011)
14. K. Bartschat, E.T. Hudson, M.P. Scott, P.G. Burke, V.M. Burke, J. Phys. B **29**, 115 (1996)
15. T.W. Gorczyca, N.R. Badnell, J. Phys. B **30**, 3897 (1997)
16. J.D. Gorfinkiel, J. Tennyson, J. Phys. B **38**, 1607 (2005)
17. L. Malegat, P. Selles, A.K. Kazansky, Phys. Rev. Lett. **85**, 4450 (2000)
18. P. Selles, L. Malegat, A.K. Kazansky, Phys. Rev. A **65**, 032711 (2002)
19. F. Citrini, L. Malegat, P. Selles, A.K. Kazansky, Phys. Rev. A **67**, 042709 (2003)
20. I. Bray, J. Phys. B **33**, 581 (2000), and references therein
21. I. Bray, D.V. Fursa, Phys. Rev. A **54**, 2991 (1996)
22. I. Bray, D.V. Fursa, J. Röder, H. Erhardt, J. Phys. B **30**, L101 (1997)
23. I. Bray, D.V. Fursa, J. Röder, H. Erhardt, Phys. Rev. A **57**, R3161 (1998)
24. I. Bray, D.V. Fursa, A.T. Stelbovics, J. Phys. B **41**, 215203 (2008)
25. A.S. Kheifets, I. Bray, Phys. Rev. A **54**, R995 (1996)
26. A.S. Kheifets, I. Bray, J. Phys. B **31**, L447 (1998)
27. A.S. Kheifets, I. Bray, Phys. Rev. A **62**, 065402 (2000)
28. A.S. Kheifets, I. Bray, Phys. Rev. A **65**, 012710 (2002)
29. A.S. Kheifets, D.V. Fursa, C.W. Hines, I. Bray, J. Colgan, M.S. Pindzola, Phys. Rev. A **81**, 023418 (2010)
30. A.S. Kheifets, D.V. Fursa, I. Bray, J. Colgan, M.S. Pindzola, Phys. Rev. A **82**, 023403 (2010)
31. I.B. Abdurakhmanov, A.S. Kadyrov, I. Bray, A.T. Stelbovics, J. Phys. B **44**, 075204 (2011)
32. I.B. Abdurakhmanov, A.S. Kadyrov, D.V. Fursa, I. Bray, A.T. Stelbovics, Phys. Rev. A **84**, 062708 (2011)
33. T.N. Rescigno, M. Baertschy, W.A. Isaacs, C.W. McCurdy, Science **286**, 2474 (1999)
34. M. Baertschy, T.N. Rescigno, W.A. Isaacs, X. Li, C.W. McCurdy, Phys. Rev. A **63**, 022712 (2001)
35. C.W. McCurdy, D.A. Horner, T.N. Rescigno, F. Martin, Phys. Rev. A **69**, 032707 (2004)
36. W. Vanroose, F. Martin, T.N. Rescigno, C.W. McCurdy, Science **310**, 1787 (2005)
37. D.A. Horner, W. Vanroose, T.N. Rescigno, F. Martin, C.W. McCurdy, Phys. Rev. Lett. **98**, 073001 (2007)
38. D.A. Horner, F. Morales, T.N. Rescigno, F. Martin, C.W. McCurdy, Phys. Rev. A **76**, R 030701 (2007)
39. F. Morales, F. Martin, D.A. Horner, T.N. Rescigno, C.W. McCurdy, J. Phys. B **42**, 134013 (2009)
40. A.S. Kadyrov, I. Bray, A.M. Mukhamedzhanov, A.T. Stelbovics, Phys. Rev. Lett. **101**, 230405 (2008)
41. A.S. Kadyrov, I. Bray, A.M. Mukhamedzhanov, A.T. Stelbovics, Ann. Phys. **324**, 1516 (2009)
42. R.D. Cowan, *The Theory of Atomic Structure and Spectra* (University of California Press, Berkeley, 1981)
43. M.B. Shah, D.S. Elliott, H.B. Gilbody, J. Phys. B **20**, 3501 (1987)
44. I. Bray, A.T. Stelbovics, Phys. Rev. Lett. **70**, 746 (1993)
45. D. Kato, S. Watanabe, Phys. Rev. Lett. **74**, 2443 (1995)
46. K. Bartschat, I. Bray, J. Phys. B **29**, L577 (1996)

47. D.C. Griffin, C.P. Ballance, M.S. Pindzola, F. Robicheaux, S.D. Loch, J.A. Ludlow, M.C. Witthoeft, J. Colgan, C.J. Fontes, D.R. Schultz, J. Phys. B **38**, L199 (2005)
48. M.C. Witthoeft, M.S. Pindzola, J. Colgan, Phys. Rev. A **67**, 032713 (2003)
49. J. Colgan, M.S. Pindzola, F. Robicheaux, Phys. Rev. A **66**, 012718 (2002)
50. M.S. Pindzola, F. Robicheaux, Phys. Rev. A **61**, 052707 (2000)
51. J. Colgan, M.S. Pindzola, G. Childers, M.A. Khakoo, Phys. Rev. A **73**, 042710 (2006)
52. R.G. Montague, M.F.A. Harrison, A.C.H. Smith, J. Phys. B **17**, 3295 (1984)
53. M.B. Shah, D.S. Elliott, P. McCallion, H.B. Gilbody, J. Phys. B **21**, 2751 (1988)
54. J. Colgan, M.S. Pindzola, Phys. Rev. A **66**, 062707 (2002)
55. M.S. Pindzola, D.M. Mitnik, J. Colgan, D.C. Griffin, Phys. Rev. A **61**, 052712 (2000)
56. J. Colgan, M.S. Pindzola, D.M. Mitnik, D.C. Griffin, Phys. Rev. A **63**, 062709 (2001)
57. J. Colgan, M.S. Pindzola, D.M. Mitnik, D.C. Griffin, I. Bray, Phys. Rev. Lett. **87**, 213201 (2001)
58. M.S. Pindzola, F. Robicheaux, N.R. Badnell, T.W. Gorczyca, Phys. Rev. A **56**, 1994 (1997)
59. J. Colgan, S.D. Loch, M.S. Pindzola, C.P. Ballance, D.C. Griffin, Phys. Rev. A **68**, 032712 (2003)
60. J.C. Berengut, S.D. Loch, M.S. Pindzola, C.P. Ballance, D.C. Griffin, Phys. Rev. A **76**, 042714 (2007)
61. T.-G. Lee, S.D. Loch, C.P. Ballance, J.A. Ludlow, M.S. Pindzola, Phys. Rev. A **82**, 042721 (2010)
62. M.S. Pindzola, J. Colgan, F. Robicheaux, D.C. Griffin, Phys. Rev. A **62**, 042705 (2000)
63. J.A. Ludlow, S.D. Loch, M.S. Pindzola, C.P. Ballance, D.C. Griffin, M.E. Bannister, M. Fogle, Phys. Rev. A **78**, 052708 (2008)
64. C.P. Ballance, S.D. Loch, J.A. Ludlow, Sh.A. Abdel-Naby, M.S. Pindzola, Phys. Rev. A **84**, 062713 (2011)
65. C.P. Ballance, D.C. Griffin, J.A. Ludlow, M.S. Pindzola, J. Phys. B **37**, 4779 (2004)
66. J.A. Ludlow, C.P. Ballance, S.D. Loch, M.S. Pindzola, D.C. Griffin, Phys. Rev. A **79**, 032715 (2009)
67. N.R. Badnell, M.S. Pindzola, I. Bray, D.C. Griffin, J. Phys. B **31**, 911 (1998)
68. S.D. Loch, C.P. Ballance, D. Wu, Sh.A. Abdel-Naby, M.S. Pindzola, J. Phys. B **45**, 065201 (2012)
69. D.C. Griffin, D.M. Mitnik, J. Colgan, M.S. Pindzola, Phys. Rev. A **64**, 032718 (2001)
70. M.C. Witthoeft, J. Colgan, M.S. Pindzola, Phys. Rev. A **68**, 022711 (2003)
71. C.P. Ballance, D.C. Griffin, J. Colgan, S.D. Loch, M.S. Pindzola, Phys. Rev. A **68**, 062705 (2003)
72. E. Schow, K. Hazlett, J.G. Childers, C. Medina, G. Vitug, I. Bray, D.V. Fursa, M.A. Khakoo, Phys. Rev. A **72**, 062717 (2005)
73. J. Colgan, M.S. Pindzola, F.J. Robicheaux, D.C. Griffin, M. Baertschy, Phys. Rev. A **65**, 042721 (2002)
74. J. Colgan, M.S. Pindzola, Phys. Rev. A **74**, 012713 (2006)
75. J. Colgan, M. Foster, M.S. Pindzola, I. Bray, A.T. Stelbovics, D.V. Fursa, J. Phys. B **42**, 145002 (2009)
76. J. Colgan, O. Al-Hagan, D.H. Madison, A.J. Murray, M.S. Pindzola, J. Phys. B **42**, 171001 (2009)
77. X. Ren, A. Senftleben, T. Pflüger, A. Dorn, J. Colgan, M.S. Pindzola, O. Al-Hagan, D.H. Madison, I. Bray, D.V. Fursa, J. Ullrich, Phys. Rev. A **82**, 032712 (2010)
78. X. Ren, I. Bray, D.V. Fursa, J. Colgan, M.S. Pindzola, T. Pflüger, A. Senftleben, S. Xu, A. Dorn, J. Ullrich, Phys. Rev. A **83**, 052711 (2011)
79. A.J. Murray, F.H. Read, J. Phys. B **26**, L359 (1993)
80. J.H. Macek, J.B. Sternberg, S.Y. Ovchinnikov, J.S. Briggs, Phys. Rev. Lett. **104**, 033201 (2010)
81. J.M. Feagin, J. Phys. B **44**, 011001 (2011)
82. M.S. Pindzola, F. Robicheaux, J. Colgan, J. Phys. B **38**, L285 (2005)
83. M.S. Pindzola, F. Robicheaux, S.D. Loch, J. Colgan, Phys. Rev. A **73**, 052706 (2006)
84. B. Peart, K.T. Dolder, J. Phys. B **6**, 2409 (1973)
85. H.C. Staub, P. Renault, B.G. Lindsay, K.A. Smith, R.F. Stebbings, Phys. Rev. A **54**, 2146 (2006)
86. M.S. Pindzola, Sh.A. Abdel-Naby, J.A. Ludlow, F. Robicheaux, J. Colgan, Phys. Rev. A **85**, 012704 (2012)
87. J. Colgan, M.S. Pindzola, F. Robicheaux, C. Kaiser, A.J. Murray, D.H. Madison, Phys. Rev. Lett. **101**, 233201 (2008)
88. J. Colgan, M.S. Pindzola, J. Phys.: Conf. Ser. **288**, 012001 (2011)
89. J. Colgan, O. Al-Hagan, D.H. Madison, C. Kaiser, A.J. Murray, M.S. Pindzola, Phys. Rev. A **79**, 052704 (2009)
90. O. Al-Hagan, D.H. Madison, A.J. Murray, C. Kaiser, J. Colgan, Phys. Rev. A **81**, 030701 (2010)
91. M.S. Pindzola, F. Robicheaux, J. Colgan, M.C. Witthoeft, J.A. Ludlow, Phys. Rev. A **70**, 032705 (2004)
92. M.S. Pindzola, D. Mitnik, F. Robicheaux, Phys. Rev. A **59**, 4390 (1999)
93. M.S. Pindzola, F. Robicheaux, J. Colgan, Phys. Rev. A **76**, 024704 (2007)
94. M.S. Pindzola, F. Robicheaux, J. Colgan, J. Phys. B **39**, L127 (2006)
95. D.J. Yu, S. Rachafi, J. Jureta, P. Defrance, J. Phys. B **25**, 4593 (1992)
96. B. Peart, D.S. Walton, K.T. Dolder, J. Phys. B **4**, 88 (1971)
97. M.S. Pindzola, C.P. Ballance, F. Robicheaux, J. Colgan, J. Phys. B **43**, 105204 (2011)
98. M.S. Pindzola, J.A. Ludlow, C.P. Ballance, F. Robicheaux, J. Colgan, J. Phys. B **44**, 105202 (2011)
99. M.S. Pindzola, J.A. Ludlow, F. Robicheaux, J. Colgan, D.C. Griffin, J. Phys. B **42**, 215204 (2009)
100. M.S. Pindzola, F. Robicheaux, J. Colgan, J. Phys. B **41**, 235202 (2008)
101. M. Dürr, A. Dorn, J. Ullrich, S.P. Cao, A. Czasch, A.S. Kheifets, J.R. Gotz, J.S. Briggs, Phys. Rev. Lett. **98**, 193201 (2007)
102. X. Ren, A. Dorn, J. Ullrich, Phys. Rev. Lett. **101**, 093201 (2008)
103. M.S. Pindzola, F. Robicheaux, Phys. Rev. A **57**, 318 (1998)
104. E.S. Smyth, J.S. Parker, K.T. Taylor, Comp. Phys. Commun. **114**, 1 (1998)
105. J.S. Parker, B.J.S. Doherty, K.T. Taylor, K.D. Schultz, C.I. Blaga, L.F. DiMauro, Phys. Rev. Lett. **96**, 133001 (2006)
106. J.C. Levin, G.B. Armen, I.A. Sellin, Phys. Rev. Lett. **76**, 1220 (1996)

107. J.A.R. Samson, W.C. Stolte, Z.X. He, J.N. Cutler, Y. Lu, R.J. Bartlett, Phys. Rev. A **57**, 1906 (1998)
108. K.W. Meyer, C.H. Greene, B.D. Esry, Phys. Rev. Lett. **78**, 4902 (1997)
109. U. Kleiman, T. Topcu, M.S. Pindzola, F. Robicheaux, J. Phys. B **39**, L61 (2006)
110. M.S. Pindzola, F. Robicheaux, Phys. Rev. A **58**, 4229 (1998)
111. U. Kleiman, M.S. Pindzola, F. Robicheaux, Phys. Rev. A **72**, 022707 (2005)
112. M. Foster, J. Colgan, J. Phys. B **39**, 5067 (2006)
113. J. Colgan, M.S. Pindzola, Phys. Rev. A **65**, 022709 (2002)
114. R. Wehlitz, D. Lukić, J.B. Bluett, Phys. Rev. A **71**, 012707 (2005)
115. J. Colgan, D.C. Griffin, C.P. Ballance, M.S. Pindzola, Phys. Rev. A **80**, 063414 (2009)
116. D.C. Griffin, M.S. Pindzola, C.P. Ballance, J. Colgan, Phys. Rev. A **79**, 023413 (2009)
117. J. Colgan, M.S. Pindzola, F. Robicheaux, J. Phys. B **34**, L457 (2001)
118. J. Colgan, M.S. Pindzola, Phys. Rev. A **65**, 032729 (2002)
119. J. Colgan, M.S. Pindzola, J. Phys. B **37**, 1153 (2004)
120. H. Bräuning et al., J. Phys. B **31**, 5149 (1998)
121. S. Cvejanović, J.P. Wightman, T.J. Reddish, F. Maulbetsch, M.A. MacDonald, A.S. Kheifets, I. Bray, J. Phys. B **33**, 265 (2000)
122. C. Dawson, S. Cvejanović, D.P. Seccombe, T.J. Reddish, F. Maulbetsch, A. Huetz, J. Mazeau, A.S. Kheifets, J. Phys. B **34**, L525 (2001)
123. S.A. Collins, A. Huetz, T.J. Reddish, D.P. Seccombe, K. Soejima, Phys. Rev. A **64**, 062706 (2001)
124. P. Bolognesi, R. Camilloni, M. Coreno, G. Turri, J. Berakdar, A.S. Kheifets, L. Avaldi, J. Phys. B **34**, 3193 (2001)
125. A. Knapp et al., Phys. Rev. Lett. **89**, 033004 (2002)
126. A. Knapp et al., J. Phys. B **35**, L521 (2002)
127. J. Colgan, M.S. Pindzola, Phys. Rev. A **67**, 012711 (2003)
128. G. Zhu, M. Schuricke, J. Steinmann, J. Albrecht, J. Ullrich, I. Ben-Itzhak, T.J.M. Zouros, J. Colgan, M.S. Pindzola, A. Dorn, Phys. Rev. Lett. **103**, 103008 (2009)
129. J.A. Ludlow, J. Colgan, T.G. Lee, M.S. Pindzola, F. Robicheaux, J. Phys. B **42**, 225204 (2009)
130. F. Maulbetsch, J.S. Briggs, J. Phys. B **28**, 551 (1993)
131. M.S. Pindzola, F. Robicheaux, J. Phys. B **31**, L823 (1998)
132. J. Colgan, M.S. Pindzola, Phys. Rev. Lett. **88**, 173002 (2002)
133. S.X. Hu, J. Colgan, L.A. Collins, J. Phys. B **38**, L35 (2004)
134. L.A.A. Nikolopoulos, P. Lambropoulos, J. Phys. B **34**, 545 (2001)
135. L. Feng, H.W. van der Hart, J. Phys. B **36**, L1 (2003)
136. B. Piraux, J. Bauer, S. Laulan, H. Bachau, Eur. J. Phys. D **26**, 7 (2003)
137. I.A. Ivanov, A.S. Kheifets, Phys. Rev. A **75**, 033411 (2007)
138. L.A.A. Nikolopoulos, P. Lambropoulos, J. Phys. B **40**, 1347 (2007)
139. E. Foumouo, Ph. Antoine, L. Malegat, H. Bachau, R. Shakeshaft, J. Phys. B **41**, 051001 (2008)
140. J. Feist, S. Nagele, R. Pazourek, E. Persson, B.I. Schneider, L.A. Collins, J. Burgdörfer, Phys. Rev. A **77**, 043420 (2008)
141. X. Guan, K. Bartschat, B.I. Schneider, Phys. Rev. A **77**, 043421 (2008)
142. D.A. Horner, C.W. McCurdy, T.N. Rescigno, Phys. Rev. A **78**, 043416 (2008)
143. A. Palacios, T.N. Rescigno, C.W. McCurdy, Phys. Rev. A **77**, 032716 (2008)
144. A. Palacios, T.N. Rescigno, C.W. McCurdy, Phys. Rev. A **79**, 033402 (2009)
145. R. Nepstad, T. Birkeland, M. Forre, Phys. Rev. A **81**, 063402 (2010)
146. H. Hasegawa, E.J. Takahashi, Y. Nabekawa, K. Ishikawa, K. Midorikawa, Phys. Rev. A **71**, 023407 (2005)
147. A.A. Sorokin, M. Wellhöfer, S.V. Bobashev, K. Tiedtke, M. Richter, Phys. Rev. A **75**, 051402 (2007)
148. A. Rudenko et al., Phys. Rev. Lett. **101**, 073003 (2008)
149. T. Weber et al., Phys. Rev. Lett. **92**, 163001 (2004)
150. M. Gisselbrecht, M. Lavollée, A. Huetz, P. Bolognesi, L. Avaldi, D.P. Seccombe, T.J. Reddish, Phys. Rev. Lett. **96**, 153002 (2006)
151. T. Weber et al., Nature **431**, 437 (2004)
152. T.J. Reddish, J. Colgan, P. Bolognesi, L. Avaldi, M. Gisselbrecht, M. Lavollée, M.S. Pindzola, A. Huetz, Phys. Rev. Lett. **100**, 193001 (2008)
153. J. Colgan, M.S. Pindzola, F. Robicheaux, J. Phys. B **37**, L377 (2004)
154. H. Kossmann, O. Schwarzkopf, B. Kämmerling, V. Schmidt, Phys. Rev. Lett. **63**, 2040 (1989)
155. J. Colgan, M.S. Pindzola, F. Robicheaux, Phys. Rev. Lett. **98**, 153001 (2007)
156. W. Vanroose, D.A. Horner, F. Martin, T.N. Rescigno, C.W. McCurdy, Phys. Rev. A **74**, 052702 (2006)
157. J. Colgan, M. Foster, M.S. Pindzola, F. Robicheaux, J. Phys. B **40**, 4391 (2007)
158. J.M. Feagin, J. Colgan, A. Huetz, T.J. Reddish, Phys. Rev. Lett. **103**, 033002 (2009)
159. X. Guan, K. Bartschat, B.I. Schneider, Phys. Rev. A **83**, 043403 (2011)
160. J. Colgan, M.S. Pindzola, F. Robicheaux, J. Phys. B **41**, 121002 (2008)
161. X. Guan, K. Bartschat, B.I. Schneider, Phys. Rev. A **82**, 041404 (2010)
162. X. Guan, K. Bartschat, B.I. Schneider, Phys. Rev. A **84**, 033403 (2011)
163. J. Colgan, M.S. Pindzola, F. Robicheaux, Phys. Rev. Lett. **93**, 053201 (2004)
164. R. Wehlitz, M.T. Huang, B.D. DePaola, J.C. Levin, I.A. Sellin, T. Nagata, J.W. Cooper, Y. Azuma, Phys. Rev. Lett. **81**, 1813 (1998)
165. J. Colgan, M.S. Pindzola, F. Robicheaux, Phys. Rev. A **72**, 022727 (2005)
166. J. Colgan, M.S. Pindzola, J. Phys. B **39**, 1879 (2006)
167. J. Colgan, M.S. Pindzola, Phys. Rev. Lett. **108**, 053001 (2012)
168. M.S. Pindzola, F. Robicheaux, J. Colgan, J. Phys. B **40**, 1695 (2007)
169. H. Knudsen, L.H. Andersen, P. Hvelpund, G. Astner, H. Cederquist, H. Danared, L. Liljeby, K.G. Rensfelt, J. Phys. B **17**, 3545 (1984)
170. M. Foster, J. Colgan, M.S. Pindzola, Phys. Rev. Lett. **100**, 033201 (2008)
171. P. Hvelpund et al., J. Phys. B **27**, 925 (1994)
172. L.H. Andersen et al., Phys. Rev. A **41**, 6536 (1990)

173. X. Guan, K. Bartschat, Phys. Rev. Lett. **103**, 213201 (2009)
174. H. Knudsen et al., Nucl. Instrum. Methods Phys. Res. B **267**, 244 (2009)
175. M.S. Pindzola, T.G. Lee, J. Colgan, J. Phys. B **44**, 205204 (2011)
176. M. Foster, J. Colgan, M.S. Pindzola, J. Phys. B **41**, 111002 (2008)
177. M. Foster, J. Colgan, M.S. Pindzola, J. Phys. B **42**, 149801 (2009)
178. M. Schulz, D. Fischer, R. Moshammer, J. Ullrich, J. Phys. B **38**, 1363 (2005)
179. M.S. Pindzola, F. Robicheaux, J. Colgan, Phys. Rev. A **82**, 042719 (2010)
180. J. Colgan, M.S. Pindzola, F. Robicheaux, M.F. Ciappina, J. Phys. B **44**, 175205 (2011)
181. M. Schulz, R. Moshammer, D. Fischer, H. Kollmus, D.H. Madison, S. Jones, J. Ullrich, Nature **422**, 48 (2003)
182. M. McGovern, D. Assafrão, J.R. Molhallem, C.T. Whelan, H.R.J. Walters, Phys. Rev. A **81**, 042704 (2010)
183. M.S. Pindzola, J.A. Ludlow, J. Colgan, Phys. Rev. A **80**, 032707 (2009)
184. A. Lühr, A. Saenz, Phys. Rev. A **80**, 022705 (2009)
185. M.S. Pindzola, T.G. Lee, J. Colgan, J. Phys. B **43**, 235201 (2010)
186. I. Ben-Itzhak, E. Wells, D. Studanski, V. Krishnamurthi, K.D. Carnes, H. Knudsen, J. Phys. B **34**, 1143 (2001)
187. T.G. Lee, M.S. Pindzola, J. Colgan, J. Phys. B **45**, 045203 (2012)
188. L.H. Andersen et al., J. Phys. B **23**, L395 (1990)